National Defence / Défense nationale

DISCUSSION ON THE MODELLING AND PROCESSING OF SIGNALS FROM AN ACOUSTO-OPTIC SPECTRUM ANALYZER

by

Guy Farley
Radar ESM Section
Electronic Warfare Division

DEFENCE RESEARCH ESTABLISHMENT OTTAWA
TECHNICAL NOTE 87-13

PCN
011LB11

June 1987
Ottawa

ABSTRACT

This report discusses, in its first part, the modelling of CW signals generated by an Acousto-Optic Spectrum Analyzer (AOSA). It also shows how this calculation can be related to pulse modulated signals. In its second part, it discusses the processing of those signals to detect and to estimate the carrier frequency and the power of an input radar signal. It also proposes a system block diagram to implement the former two functions.

RÉSUMÉ

La première partie de ce rapport discute le calcul des signaux générés par un analyseur de spectre acousto-optique pour des ondes continues. On montre aussi comment ce calcul peut s'appliquer à des impulsions radar. La deuxième partie de ce rapport discute le traitement de ces signaux pour détecter la présence d'un signal et pour en estimer la fréquence et la puissance. On propose aussi une façon d'effectuer ces deux premières fonctions.

TABLE OF CONTENTS

Page

ABSTRACT/RÉSUMÉ iii

TABLE OF CONTENTS v

LIST OF FIGURES vii

1.0 INTRODUCTION 1

2.0 MODEL 1
- 2.1 Continuous Wave Input Signal 3
  - 2.1.1 General case 3
  - 2.1.2 Untruncated Gaussian windowing 8
  - 2.1.3 Truncated exponential windowing 8
  - 2.1.4 Rectangular windowing 12
- 2.2 Pulse Modulated Input Signal 12

3.0 PROCESSING 19
- 3.1 Detection 19
- 3.2 Power Estimation 26
- 3.3 Carrier Frequency Estimation 28

4.0 CONCLUDING REMARKS 29

5.0 REFERENCES 31

APPENDIX I: CALCULATION OF X_{jk} FOR A CW INPUT 32

APPENDIX II: NUMERICAL CALCULATION OF $G(f)$ FOR THE GENERAL CASE . . 36

LIST OF FIGURES

Page

FIGURE 1 - ACOUSTO-OPTIC SPECTRUM ANALYZER CONFIGURATION 2
FIGURE 2 - WINDOW $w(z)$ WHEN $\alpha\tau = 0.5, T = 1$ 5
FIGURE 3 - $G(f)$ WHEN $\alpha\tau = 0.5, T = 1$ 6
FIGURE 4 - $\mathcal{H}(f)$ FOR $\alpha\tau = 0.5, T = 1, \tau B = 1$ 7
FIGURE 5 - WINDOW $w(z)$ WHEN $\alpha\tau = 0, T = 2$ 9
FIGURE 6 - $G(f)$ WHEN $\alpha\tau = 0, T = 2$ 10
FIGURE 7 - $\mathcal{H}(f)$ FOR $\alpha\tau = 0, T = 2, \tau B = 1$ 11
FIGURE 8 - WINDOW $w(z)$ WHEN $\alpha\tau = 0.5, T = 0$ 13
FIGURE 9 - $G(f)$ WHEN $\alpha\tau = 0.5, T = 0$ 14
FIGURE 10 - $\mathcal{H}(f)$ FOR $\alpha\tau = 0.5, T = 0, \tau B = 1$ 15
FIGURE 11 - WINDOW $w(z)$ WHEN $\alpha\tau = 0, T = 0$ 16
FIGURE 12 - $G(f)$ WHEN $\alpha\tau = 0, T = 0$ 17
FIGURE 13 - $\mathcal{H}(f)$ FOR $\alpha\tau = 0, T = 0, \tau B = 1$ 18
FIGURE 14 - OUTPUT OF AOSA FOR $\alpha\tau = 0, T = 0, \tau B = 3/4$ 20
FIGURE 15 - OUTPUT OF AOSA FOR $\alpha\tau = 0, T = 0, \tau B = 6$ 21
FIGURE 16 - PERFORMANCE CURVE 25
FIGURE 17 - DETECTION/ESTIMATION SYSTEM 30

1.0 INTRODUCTION

Acousto-Optic spectrum analyzers (AOSA) are viable contenders to be used as receivers for radar electronic support measures (RESM) applications especially because of their high intercept probability and their ability to handle simultaneous signals. However, they require a post-processor to extract the desired information before it is passed on to a computer for further processing. This report discusses, in the first part, the modelling of the output signal that is generated by an AOSA, and in the second part, the processing of that signal to detect the presence of a radar signal and to estimate the power and the carrier frequency of that signal.

2.0 MODEL

A block diagram of the AOSA configuration of interest in this report is shown in Figure 1. The collimated light wave generated by the laser impinges on the Bragg cell at the Bragg angle θ_B. The diffracted field distribution in the frequency plane contains the frequency analysis of the input signal. Therefore, an array of photodetectors placed at the frequency plane can be used to transform the result of this analysis, which is in the form of optical signals, into electrical signals which can be further processed and analyzed. The input signal, which is typically an electrical signal from an antenna feed, is transformed by the Bragg cell to an acoustic wave which interacts with the optical beam with the result that part of the light entering the cell is diffracted at an angle proportional to the frequency of the input signal.

The technological details and performance of the various components of this spectrum analyzer are beyond the scope of this report but are currently the object of active research. The efficiency and bandwidth of the Bragg cell, for instance, are parameters which are sought to be increased, for obvious reasons. It should be noted that the input signal is usually mixed with a local oscillator, before it is introduced to the Bragg cell, to obtain a signal within the passband of the transducer.

Theoretical formulation and experimental results of the spectrum analysis performed by this type of configuration can be found in [1]. A deeper investigation of the details of the Bragg cell diffraction patterns can be found in [2]. A mathematical model that is frequently used to describe the signal processing of this AOSA and the one that will be used throughout this report is represented by the following equation [3][4]:

$$X_{jk} = \int_{jI}^{(j+1)I} \int_{-\infty}^{\infty} H(f - f_k) \left| \int_{-\infty}^{\infty} w(z)u(t-z)\exp(-i2\pi fz)dz \right|^2 df\, dt \qquad (1)$$

where X_{jk} is the voltage produced at the output of the k^{th} detector for the j^{th} time frame. In this equation, $u(t)$ is the input signal, $w(z)$ is the window function determined by the Bragg cell and the shaping of the laser beam, f_k is the frequency associated with the k^{th} detector, $H(f)$ is a spectral weighting function that describes the spatial response of an individual detector element and I is the integration time of the detectors. This equation implies that the instantaneous light intensity distribution shining on the array of photodetectors is the instantaneous magnitude squared of the Fourier transform of the signals propagating across the Bragg cell. Each photodetector in the focal plane spatially integrates the light intensity distribution and converts it to currents which are integrated and sampled during periodic intervals.

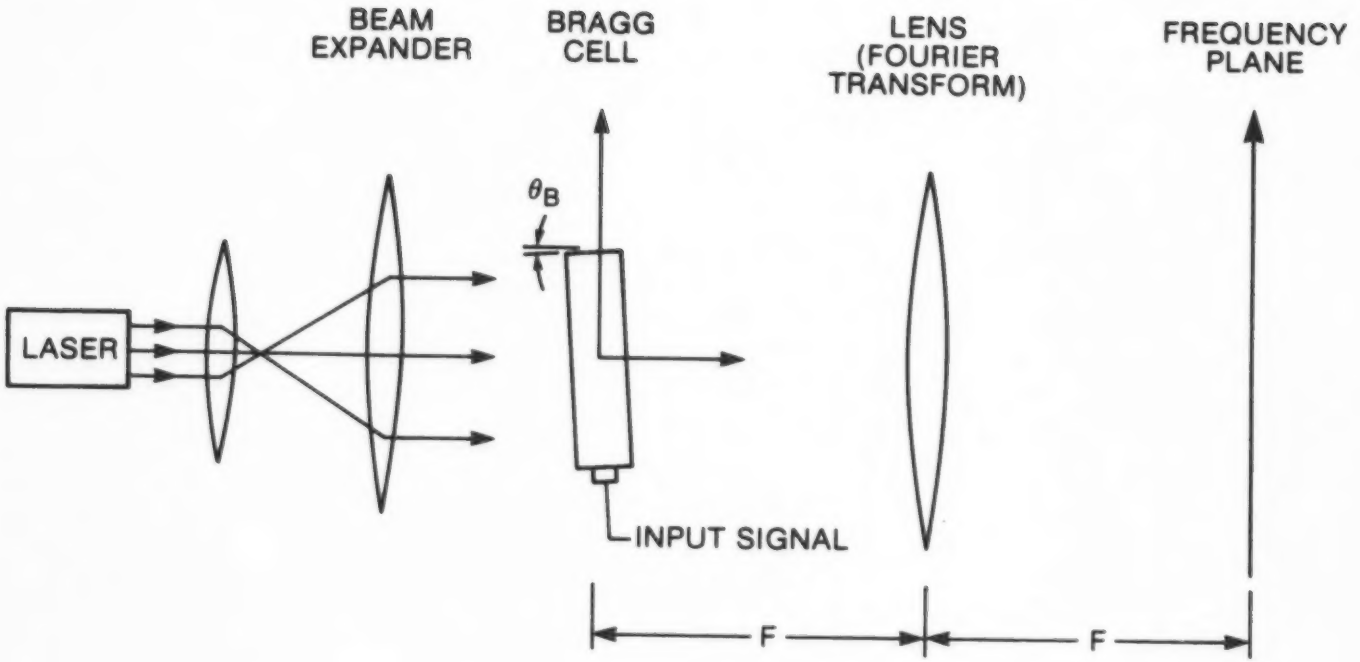

FIGURE 1 - ACOUSTO-OPTIC SPECTRUM ANALYZER CONFIGURATION

2.1 Continuous Wave Input Signal

For a sinusoidal input, $u(t) = A\cos(2\pi f_0 t + \phi)$, it can be shown (see Appendix I) that

$$X_{jk} = \frac{A^2 I}{4}\mathcal{H}(f_k - f_0) \tag{2}$$

where $\mathcal{H}(f)$ is the convolution between the functions G and H,

$$\mathcal{H}(f) = \int_{-\infty}^{\infty} H(f - f')G(f')df' \tag{3}$$

where $G(f)$ is the magnitude squared of the Fourier transformed window function,

$$G(f) = \left|\int_{-\infty}^{\infty} w(z)\exp(-i2\pi f z)dz\right|^2 \tag{4}$$

In this report, it will be assumed that $H(f)$ is a rectangular function of unit amplitude and width B Hz, symmetrical about $f = 0$. As it was mentioned before, $H(f)$ is in fact a spatial weighting function describing the response of an individual photodetector, but there is a linear one-to-one correspondence between the spatial and spectral responses due to the fact that the angle of diffraction is proportional to the frequency of the input signal. Although we assume $H(f)$ to be a rectangular function, the calculations done in this report could easily be redone for any arbitrary known $H(f)$.

2.1.1 General case

From [5] we have that the window function $w(z)$ can be described by the following equation:

$$w(z) = \exp\left[-\alpha(f_0)z - 4T^2\left(\frac{z}{\tau} - \frac{1}{2}\right)^2\right]\text{rect}\left(\frac{z}{\tau} - \frac{1}{2}\right) \tag{5}$$

where α (in nepers/sec) accounts for the acoustic amplitude attenuation and is a function of the input signal frequency, T is the ratio of the truncated aperture over the e^{-2} intensity width of the Gaussian profile, and τ (in seconds) is the transit time of the acoustic wave across the Bragg cell aperture.

If $\alpha = 0$ (that is, if we assume that there are no propagation losses in the Bragg cell), we have that $w(z)$ is a truncated Gaussian profile. To see the effect of the acoustic attenuation on the window function, we can transform equation (5) into the following form:

$$w(z) = \exp\left[-4T^2\left(\frac{z}{\tau} - \frac{1}{2} + \frac{\alpha\tau}{8T^2}\right)^2 + \frac{(\alpha\tau)^2}{16T^2} - \frac{\alpha\tau}{2}\right]\text{rect}\left(\frac{z}{\tau} - \frac{1}{2}\right) \tag{6}$$

where we can see that the acoustic attenuation causes a shift in the peak position of the Gaussian profile as well as a decrease in the peak amplitude. However, the general shape of the window function is preserved.

In general, there is no closed form solution to the Fourier transform of equation (5). So unless some simplification or approximation is done, we cannot obtain a closed form solution to $G(f)$. However, once we obtain $G(f)$ we can easily obtain $\mathcal{H}(f)$ by numerically integrating $G(f)$ over finite periods since we assume that $H(f)$ is a rectangular weighting function.

In Appendix II we show how the rectangular rule for numerical integration can be used to obtain an aliased version of $G(f)$. The resulting normalized numerical equation is:

$$G_a(v) = \tau^2 \left\{ [Re\,(K(v))]^2 + [Im\,(K(v))]^2 \right\} \tag{7}$$

where $v = f\tau$ and

$$K = \frac{\sum_{n=0}^{N-1} \left[w\left(\frac{n\tau}{N}\right) \cos\left(\frac{2\pi v n}{N}\right) - iw\left(\frac{n\tau}{N}\right) sin\left(\frac{2\pi v n}{N}\right) \right]}{N} \tag{8}$$

where N is the number of points from $w(z)$ that will be used to calculate one sample of $G(f)$. We see that the above algorithm is closely related to the DFT algorithm except for the fact that it can be used to obtain samples of $G(f)$ at any frequency instead of obtaining those for a fixed set of frequencies. Normalizing $w(z)$ to the following equation:

$$w(x) = \exp\left[-Lx - 4T^2 \left(x - \frac{1}{2} \right)^2 \right] \text{rect}\left(x - \frac{1}{2} \right) \tag{9}$$

where $L = \alpha\tau$ and $x = \frac{t}{\tau}$, makes it easy to calculate equation (7). $G_a(v)$ is periodic with a period of N with respect to v, so it should only be used to calculate samples of $G(v)$ for the range $\frac{-N}{2} < v < \frac{N}{2}$. Since $G_a(f)$ is an aliased version of $G(f)$, N should be made large enough to make this error insignificant and we should not attempt to calculate samples of $G(f)$ which are lower than a certain value. The value of N and the lowest value of $G(f)$ that we attempt to calculate using $G_a(v)$ depend on $G(f)$, so determining this may require some trial and error. When $\alpha = 0$ and $T = 0$, $w(z)$ is simply a rectangular window and $G(f)$ is a squared Sinc function. For that case, the sidelobe level is down approximately 50 dB from the peak at a frequency of $\frac{100}{\tau}$. For all other cases, the sidelobes will decrease even more rapidly.

Figure 2 shows the window function, $w(z)$, for the case of $\alpha\tau = 0.5$, $T = 1$. Figure 3 shows the function $G(f)$ calculated from equation (7) using $N = 200$ for the same case of $\alpha\tau = 0.5$, $T = 1$. Finally, Figure 4 shows $\mathcal{H}(f)$ for that same case assuming the photodetectors have a bandwidth of $B = \frac{1}{\tau}$. It should be noted that $\mathcal{H}(f)$ is symmetrical about $f = 0$ even though this is not shown on Figure 4. This last Figure is the result of numerically integrating the function $G(f)$. For that reason it is useful to have a numerical algorithm that can calculate samples of $G(f)$ at any frequency because most numerical integration programs require a function which can do that.

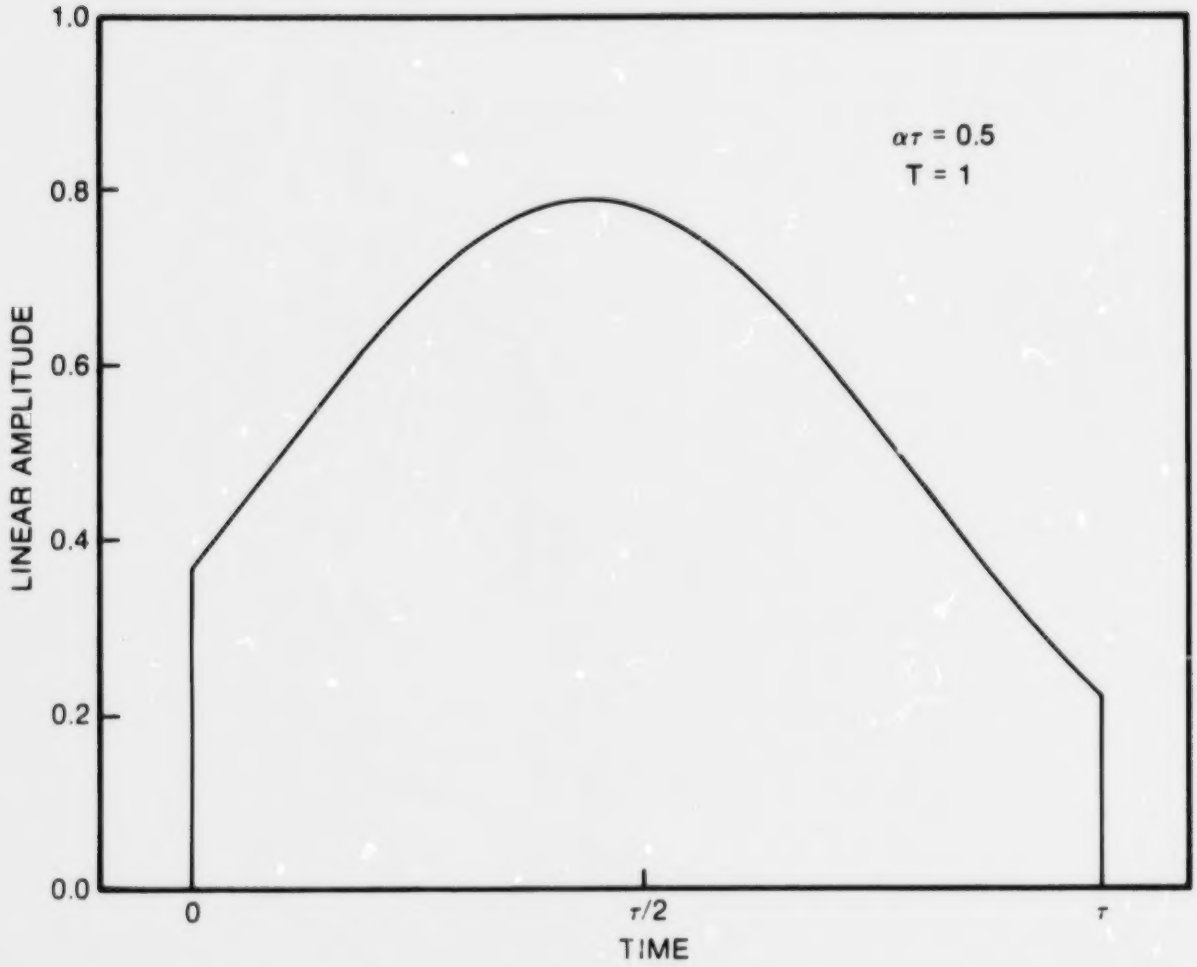

FIGURE 2 - WINDOW $w(z)$ WHEN $\alpha\tau = 0.5$, $T = 1$

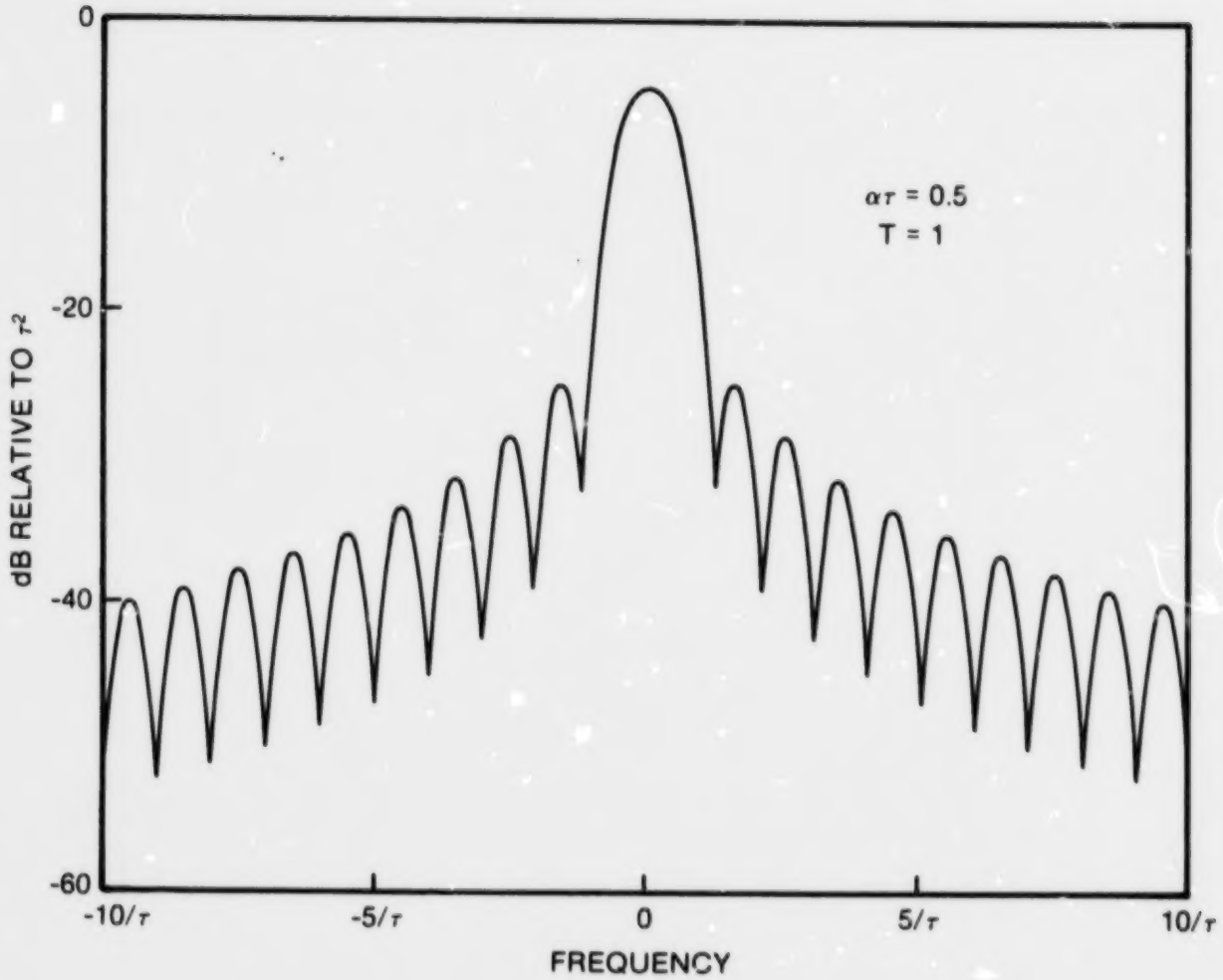

FIGURE 3 - $G(f)$ WHEN $\alpha\tau = 0.5$, $T = 1$

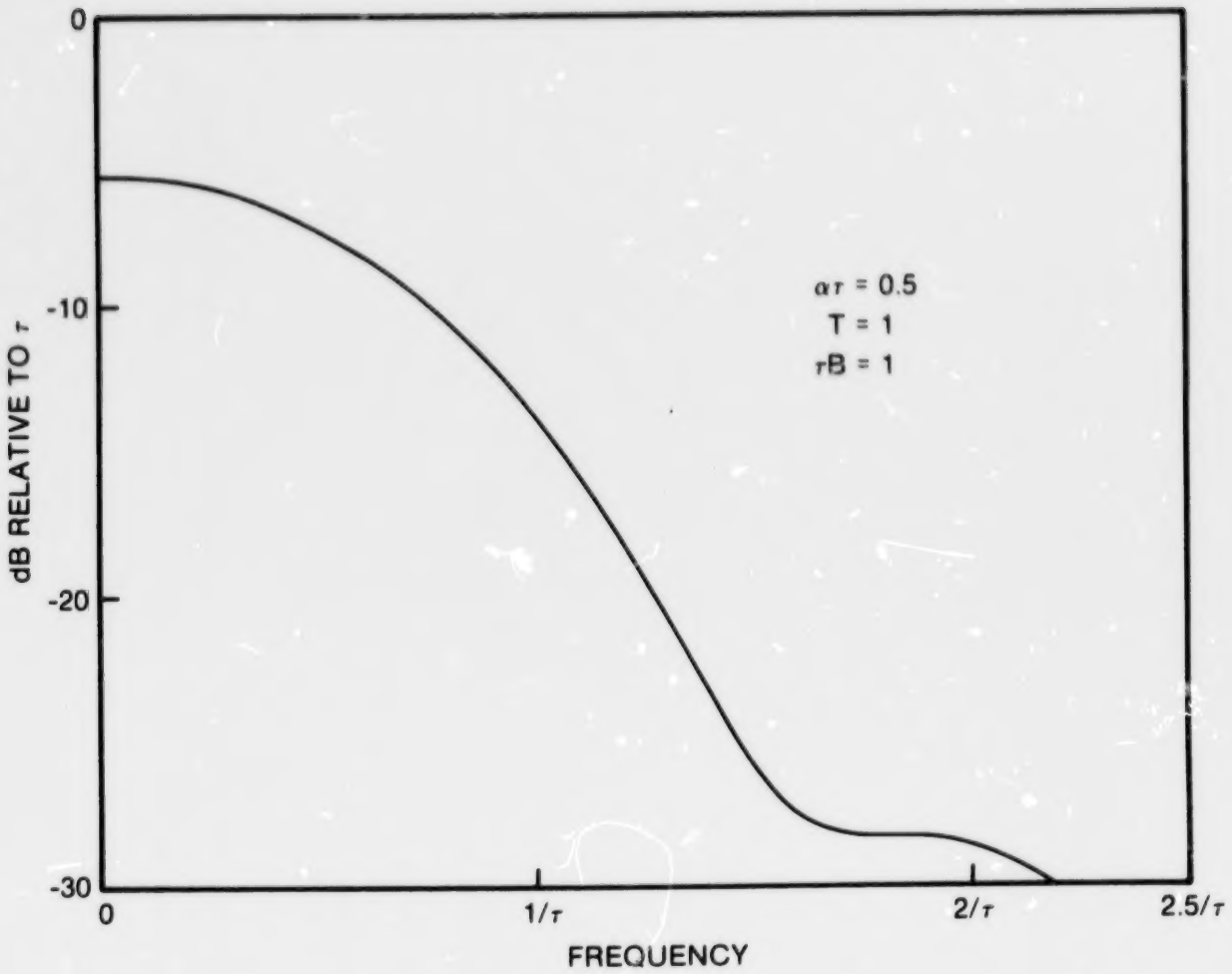

FIGURE 4 - $\mathcal{H}(f)$ FOR $\alpha\tau = 0.5$, $T = 1$, $\tau B = 1$

2.1.2 Untruncated Gaussian windowing

The preceding section showed how the output of the AOSA could be calculated using an algorithm closely related to the DFT algorithm. But it has long been recognized that the DFT is computationally expensive. In fact it is presumed that Carl Friedrich Gauss, the eminent German mathematician, developed an algorithm that could simplify its calculation as early as the year 1805 [6].

It is therefore worthwhile to note that if we assume that $\alpha = 0$ and that the Gaussian shaping is not truncated by the physical size of the Bragg cell, then we can get a closed form expression for $G(f)$. Harms and Hummels have used this result in [4] and have calculated the transform of $w(z)$ by means of a line integral in the complex plane.

If we let

$$w(z) = \exp\left[-4T^2\left(\frac{z}{\tau} - \frac{1}{2}\right)^2\right] \tag{10}$$

then

$$G(v) = \tau^2 \frac{\pi}{4T^2} \exp\left(\frac{-\pi^2 v^2}{2T^2}\right) \tag{11}$$

where again $v = f\tau$. This greatly simplifies the calculation of $\mathcal{H}(f)$ but it should only be used when T is large. In [4] this approximation for $T = 1.63$ is used and it is claimed that the resultant error is negligible.

Figure 5 shows the window function, $w(z)$, for the case of $T = 2$ while Figure 6 shows the function $G(f)$ calculated using equation (11). Finally, Figure 7 shows $\mathcal{H}(f)$ for that same case assuming the photodetectors have a bandwidth of $B = \frac{1}{\tau}$.

2.1.3 Truncated exponential windowing

If we assume that $T = 0$, that is, if we assume that the laser has no Gaussian shaping but we still want to take into account the fact that there is attenuation of the acoustic wave as it propagates through the Bragg cell, then $w(z)$ becomes:

$$w(z) = \exp(-\alpha z)\,\mathrm{rect}\left(\frac{z}{\tau} - \frac{1}{2}\right) \tag{12}$$

and it is easy to show through simple integration that:

$$G(v) = \tau^2 \frac{\left[1 - 2e^{-L}\cos(2\pi v) + e^{-2L}\right]}{L^2 + (2\pi v)^2} \tag{13}$$

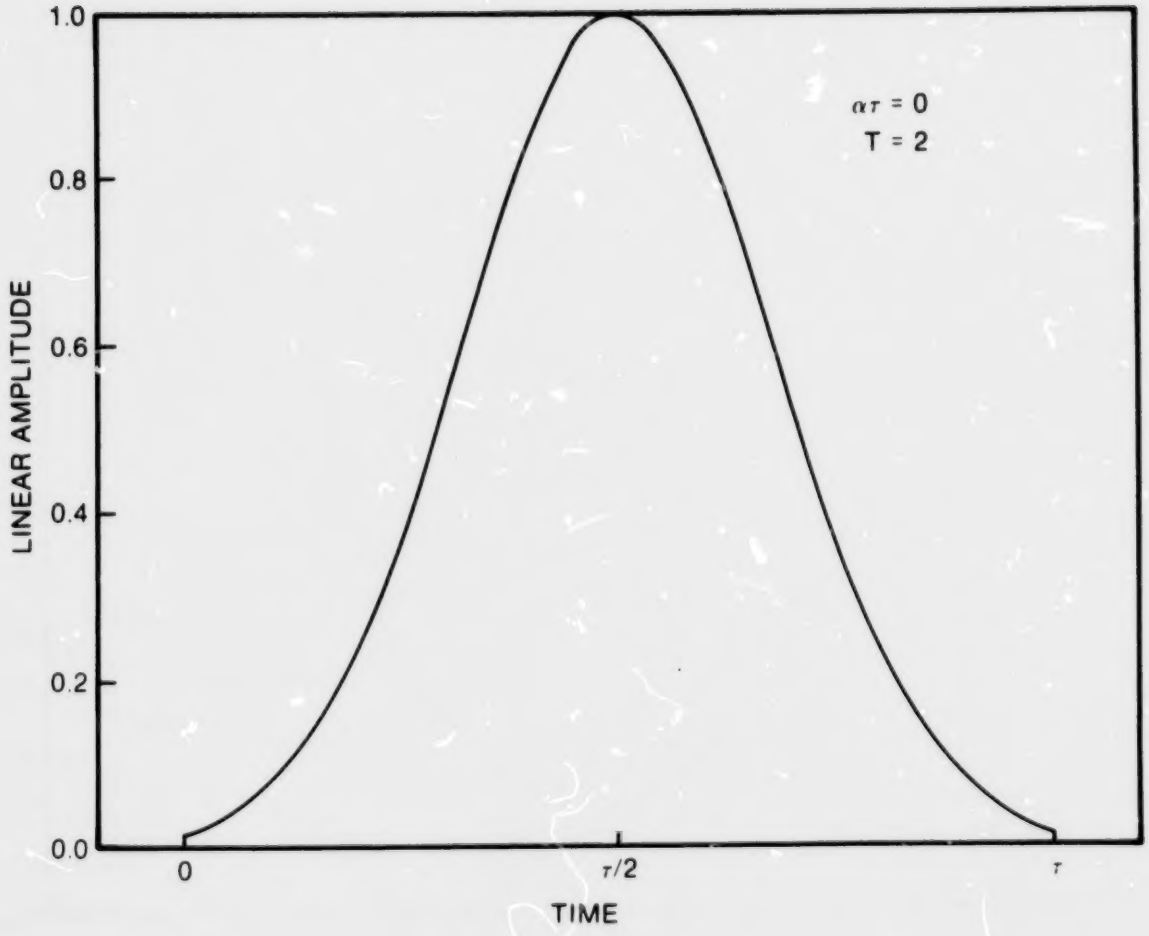

FIGURE 5 - WINDOW $w(z)$ WHEN $\alpha\tau = 0$, $T = 2$

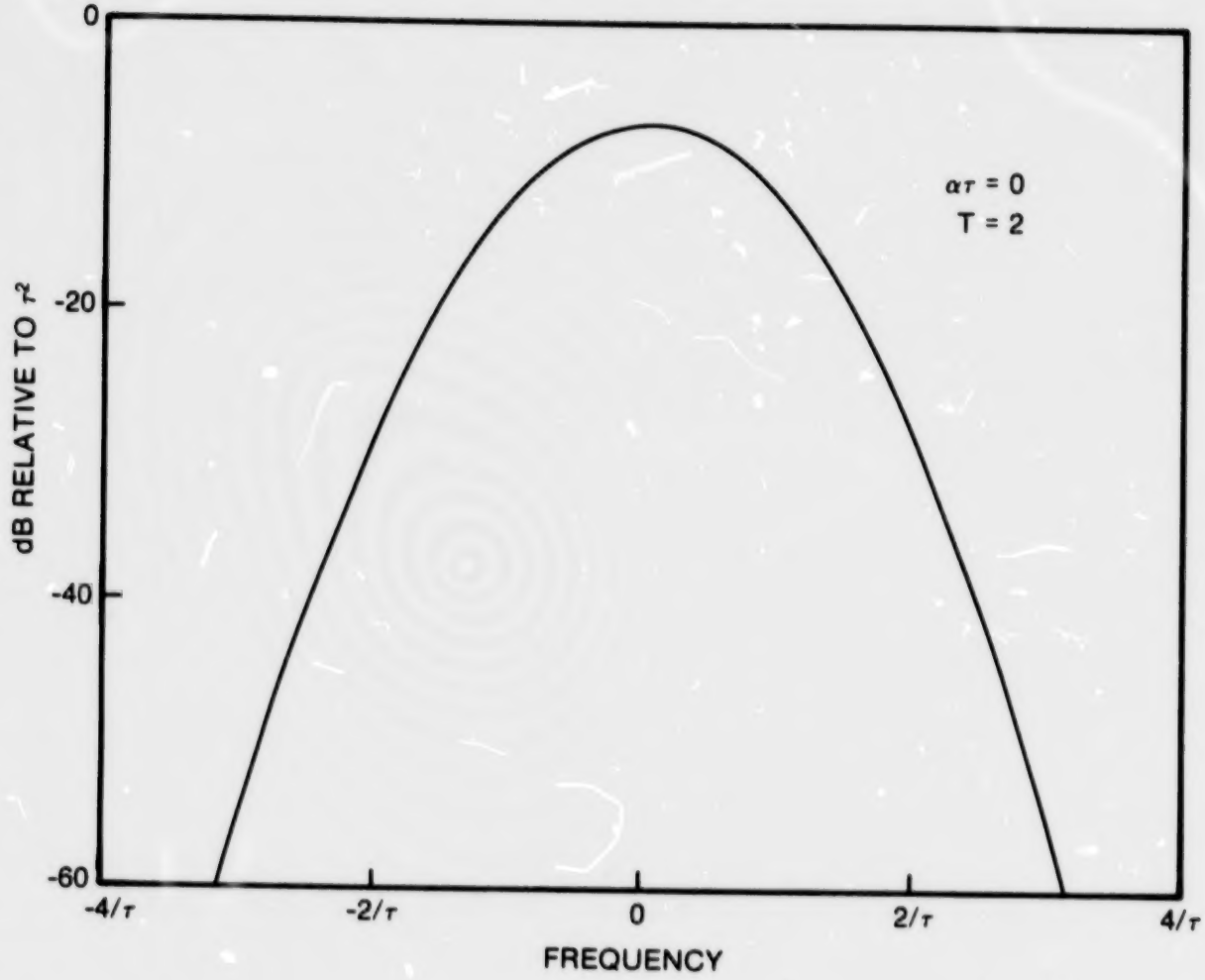

FIGURE 6 - $G(f)$ WHEN $\alpha\tau = 0$, $T = 2$

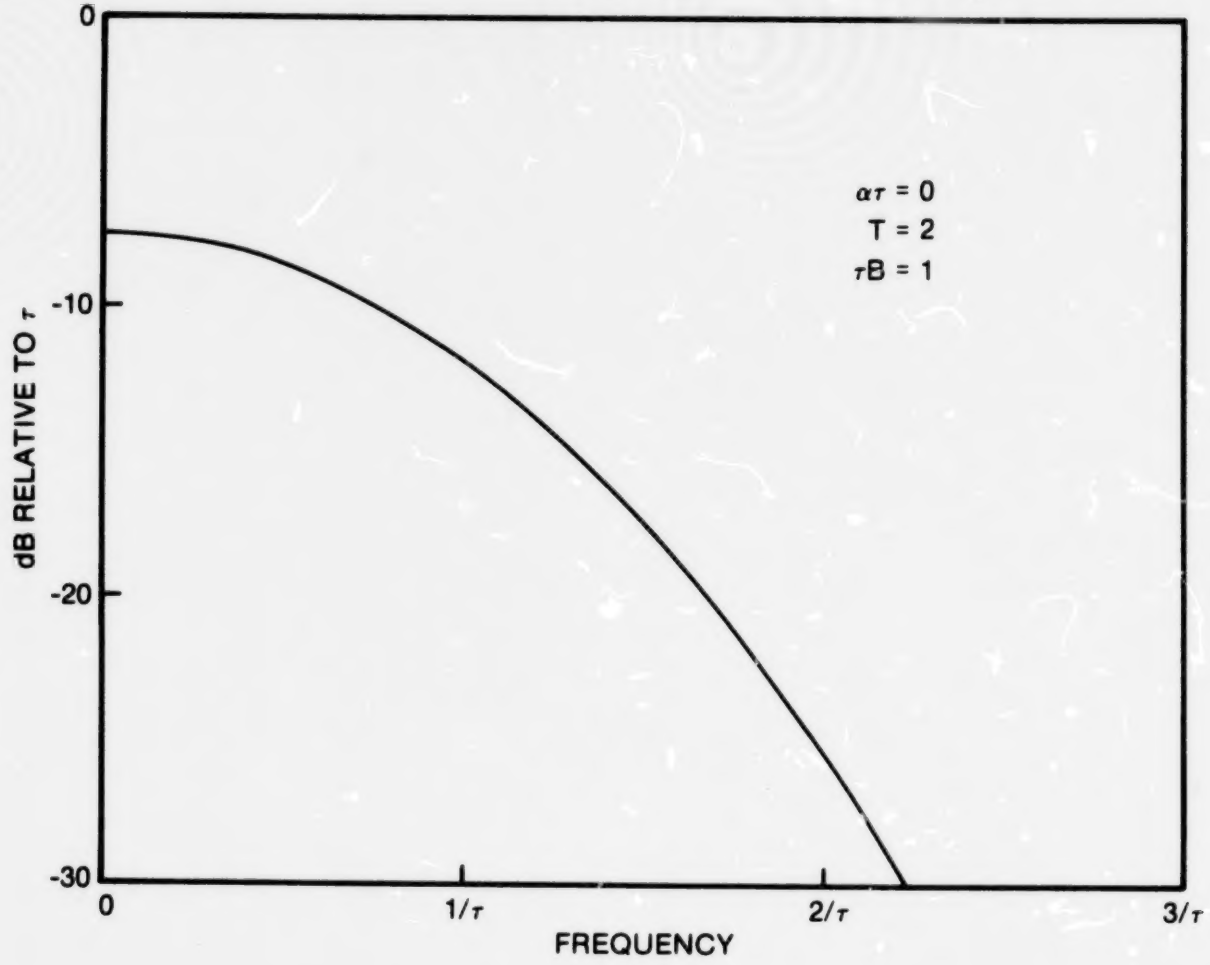

FIGURE 7 - $\mathcal{H}(f)$ FOR $\alpha\tau = 0$, $T = 2$, $\tau B = 1$

Figure 8 shows the window function, $w(z)$, for the case of $\alpha\tau = 0.5$ while Figure 9 shows the function $G(f)$ calculated using equation (13). Finally, Figure 10 shows $\mathcal{H}(f)$ for that same case assuming the photodetectors have a bandwidth of $B = \frac{1}{\tau}$.

2.1.4 Rectangular windowing

As it was mentioned earlier, if we ignore the acoustic loss of the Bragg cell and the Gaussian shaping of the laser, then $w(z)$ is simply a rectangular window whose duration is determined by the physical size of the crystal or the width of the light wave impinging on the cell. For that case it is easy to show that $w(z)$ is as shown in Figure 11 and $G(f)$ is given by the following equation:

$$G(f) = \tau^2 \frac{sin^2(2\pi f\tau/2)}{(2\pi f\tau/2)^2} \tag{14}$$

which is shown in Figure 12. The resulting function $\mathcal{H}(f)$ for $\tau B = 1$ is shown in Figure 13.

2.2 Pulse Modulated Input Signal

The preceding section has dealt with the case where the input is a sinusoidal signal or what is also called a continuous wave (CW) input signal, in the radar context. However, most radar signals are pulse modulated and one might ask how relevant is the preceding section.

It turns out that this depends on the relationship between the duration of the window function, τ, the integration time of the photodetectors, I, and the pulse width of the radar signal. For example, if the width of the radar pulse is several times larger than τ and I, then the results of the preceding section are perfectly valid to describe the outputs from the photodetectors for most of the integration time frames occurring during the pulse.

One might ask about the other extreme when the width of the radar pulse is smaller than τ. Lee [1] has done some useful calculations in that respect. There it is mentioned that there are two general effects of the window function on the time-integrated illumination pattern shining on the photodetectors:

(1) a broadening effect on the main-lobe width

which inevitably implies an increase of the side-lobe rolloff, and

(2) a smoothing effect on the side-lobe structure.

It should be noted that the integration time used in [1] was variable and was equal to the total duration of time for which the pulse is propagating through the cell and interacting with the light wave. But the interesting result is that when the width of the pulse is equal to $\tau/4$ or smaller, then the time-integrated illumination pattern can be very closely approximated by a Sinc^2 function with the first zero located at $1/PW$, where PW = pulse width.

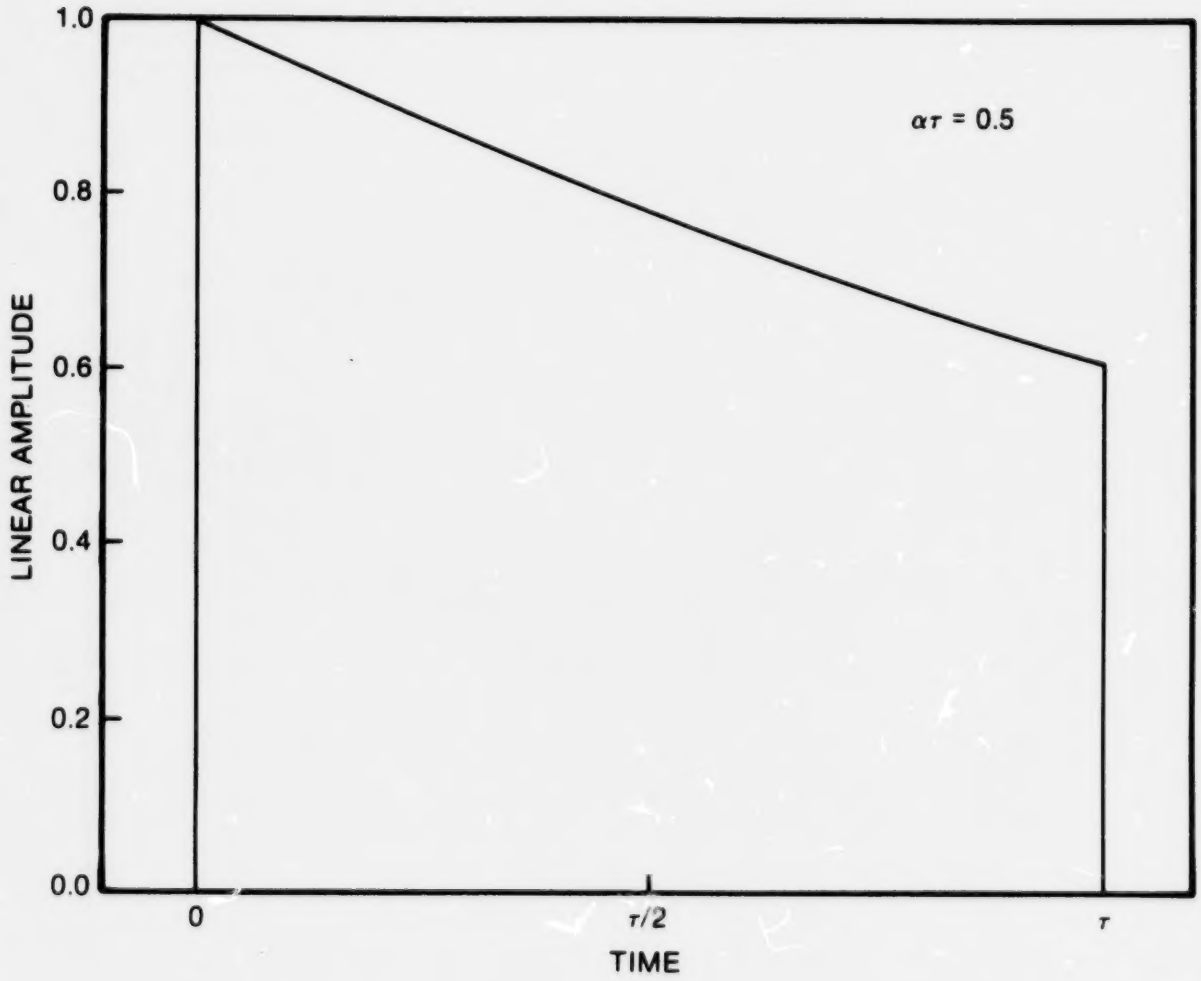

FIGURE 8 - WINDOW $w(z)$ WHEN $\alpha\tau = 0.5$, $T = 0$

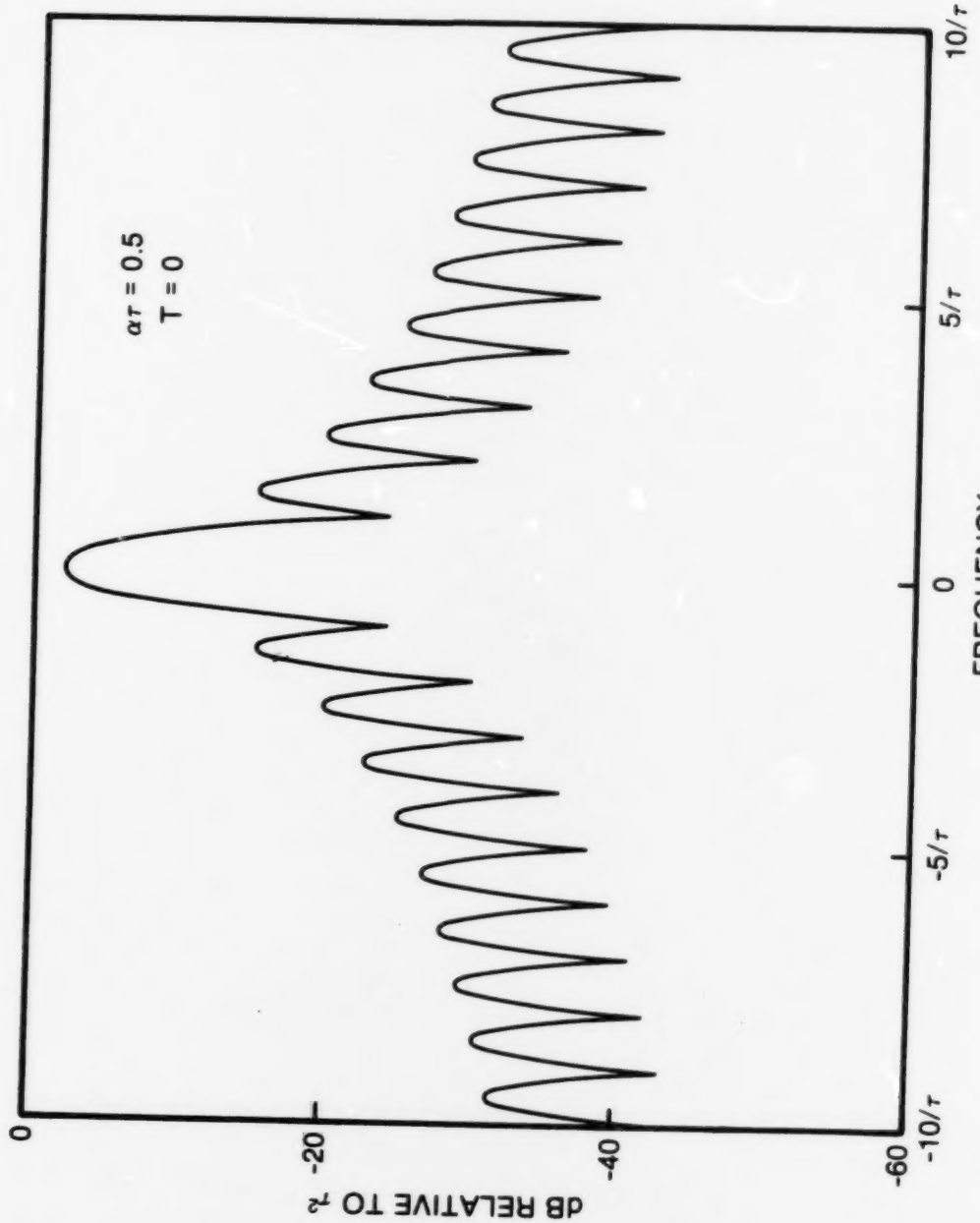

FIGURE 9 - $G(f)$ WHEN $\alpha\tau = 0.5$, $T = 0$

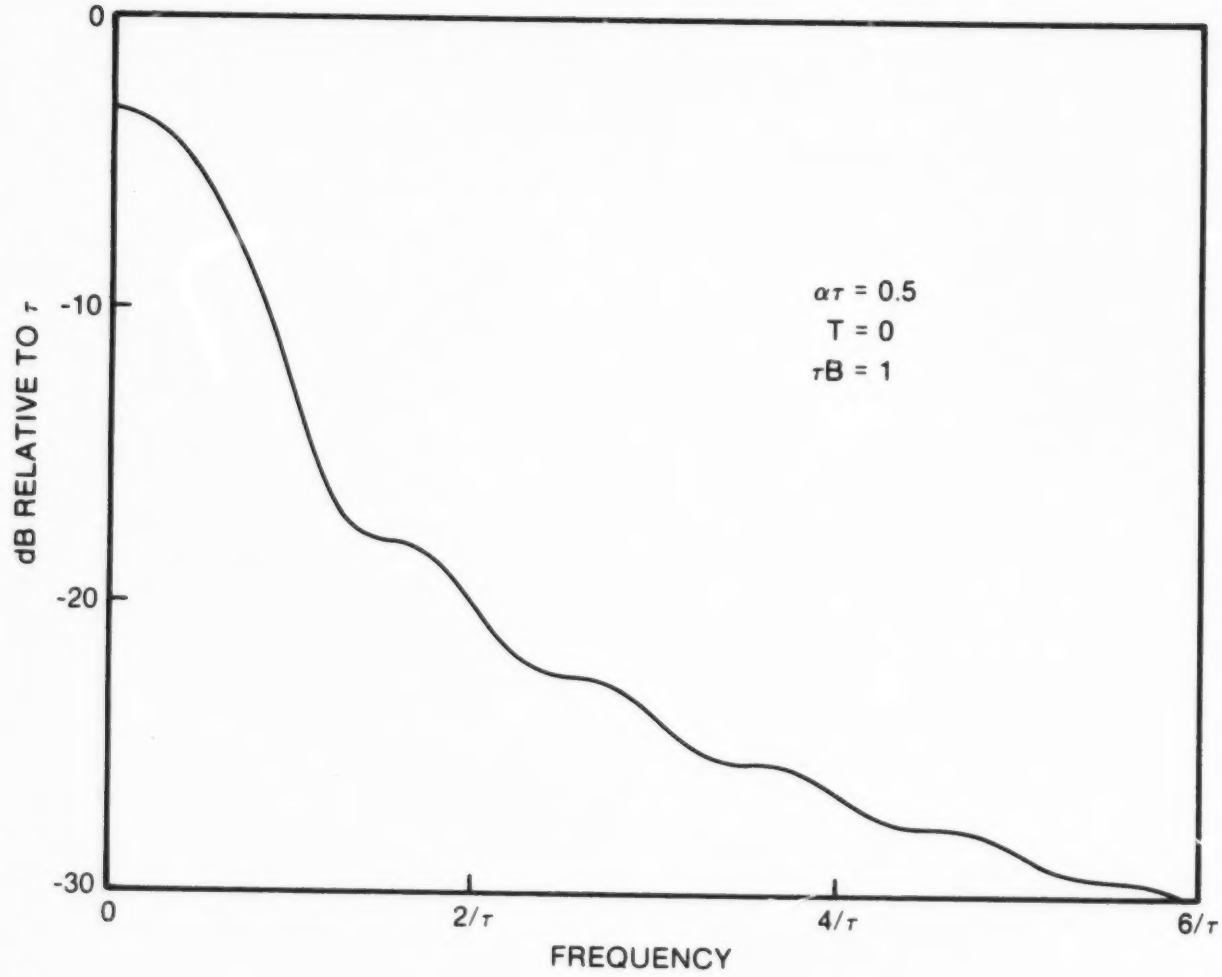

FIGURE 10 - $\mathcal{H}(f)$ FOR $\alpha\tau = 0.5$, $T = 0$, $\tau B = 1$

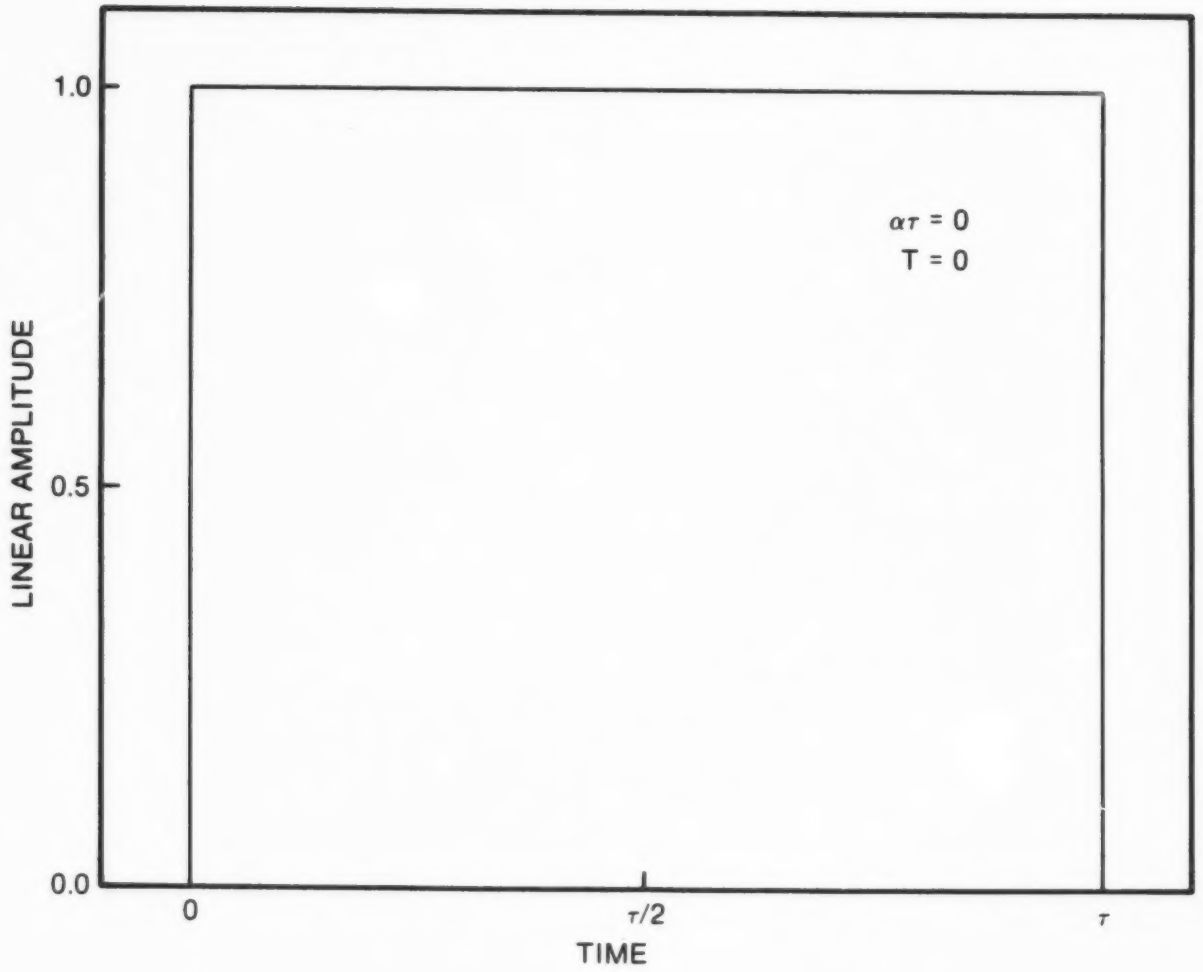

FIGURE 11 - WINDOW $w(z)$ WIIEN $\alpha\tau = 0$, $T = 0$

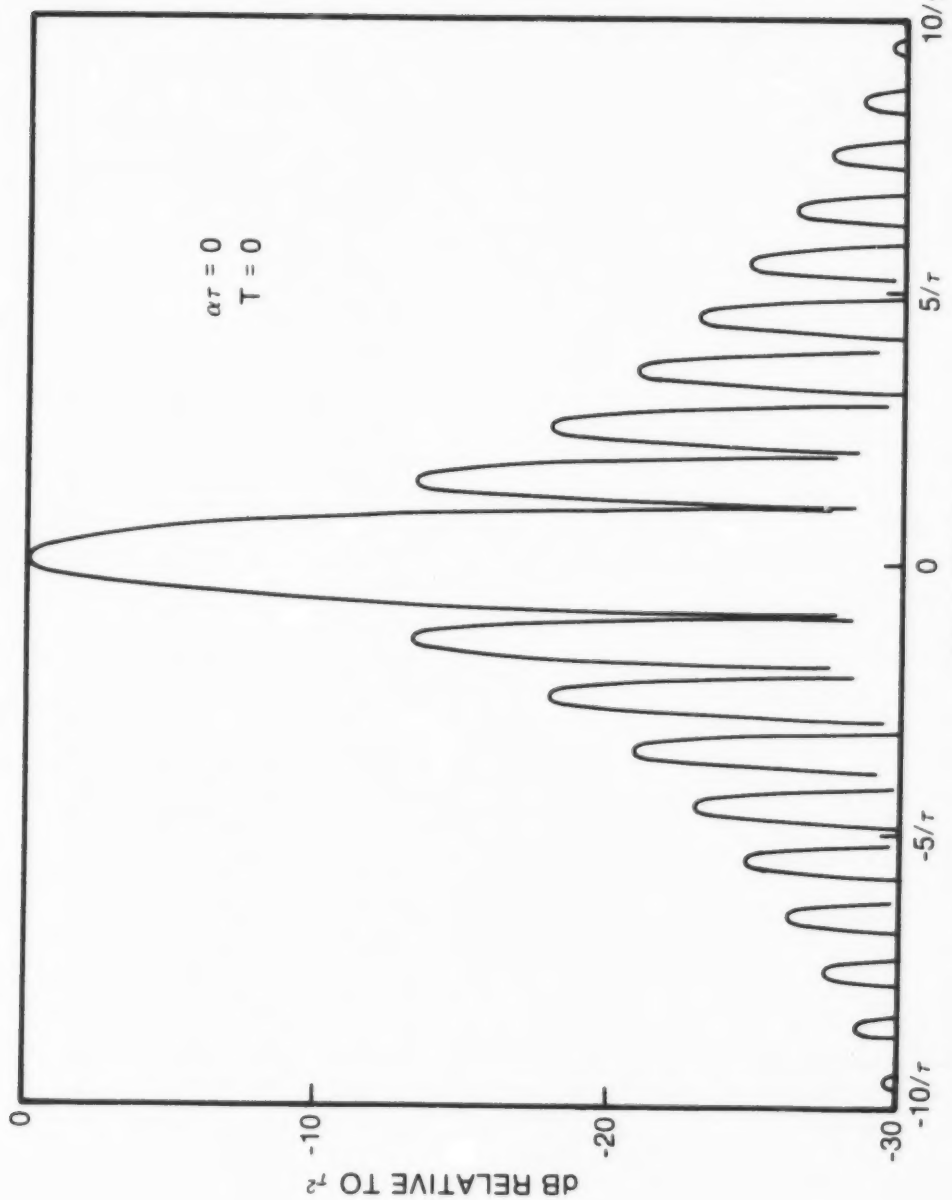

FIGURE 12 - $G(f)$ WHEN $\alpha\tau = 0$, $T = 0$

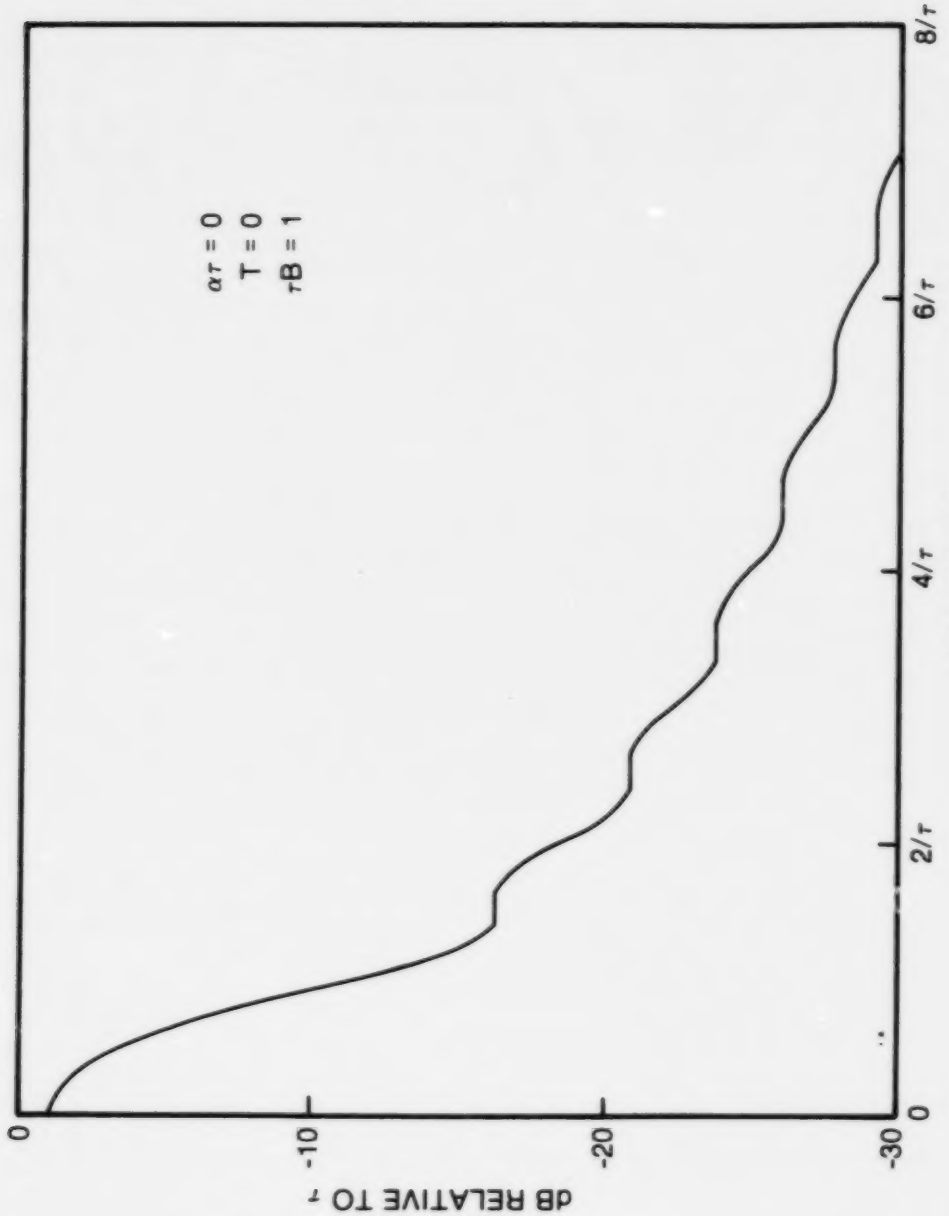

FIGURE 13 - $\mathcal{H}(f)$ FOR $\alpha\tau = 0$, $T = 0$, $\tau B = 1$

We can therefore get an appreciation of the validity conditions for the results of the previous section. Basically, the spectrum of the input signal is unaffected by the window function, $w(z)$, when the width of the radar pulse is smaller than $\tau/4$ and it is greatly affected by it, in the way that it was described in the previous section, when the width of the radar pulse is larger than τ.

3.0 PROCESSING

The preceding section has shown how we can calculate $\mathcal{H}(f)$ for different system parameters. Of course, once we have $\mathcal{H}(f)$ it becomes easy to calculate the outputs of the AOSA because these two are related as shown in equation (2). As an example, the outputs of the AOSA are shown in Figures 14 and 15 for an input signal $u(t) = A\cos(2\pi f_0 t + \phi)$. Figure 14 shows the output when $\tau B = 3/4$ for the case where $w(z)$ is a rectangular function. Figure 15 shows the output when $\tau B = 6$ for that same case. Both of these Figures show the output when f_0 corresponds to one f_k as well as when f_0 is exactly in the middle of two f_k's.

In this section, we deal with the processing of the outputs of an AOSA to detect the presence of a signal and to estimate the power and frequency of that input signal. We will approach these three problems using classical detection/estimation theory as expounded by Van Trees [7].

3.1 Detection

If we let $\bar{R} = \{r_1, r_2, r_3, ..., r_N\}$ be the received vector where the r_i's are the pixel output values for a given frame, then we can consider this problem as a binary hypothesis test:

$$\begin{aligned} H_0 &: r_i = n_i \\ H_1 &: r_i = m_i + n_i, \qquad i = 1, 2, 3, ..., N \end{aligned} \tag{15}$$

where the n_i's are assumed to be independent, zero-mean, Gaussian random variables with variance σ^2 and the m_i's are defined by

$$m_i = \frac{A^2 I}{4}\mathcal{H}_i \tag{16}$$

where the $\mathcal{H}_i$'s are the samples from $\mathcal{H}(f)$ which correspond to the pixel values of our given system.

We will assume for now that the $\mathcal{H}_i$'s are known. That is, we are seeking a test to decide whether a particular signal is present or not. Even though we use a notation which is consistent with the previous section, the following analysis is more general and applies to the detection of other signals which have not been dealt with in that section.

In practice, the noise distributions will not have a mean of zero but will rather be characterized by what is often called "fixed pattern noise". However, as is shown in [8], it is easy to determine the means and subtract them so that this zero-mean assumption is reasonable.

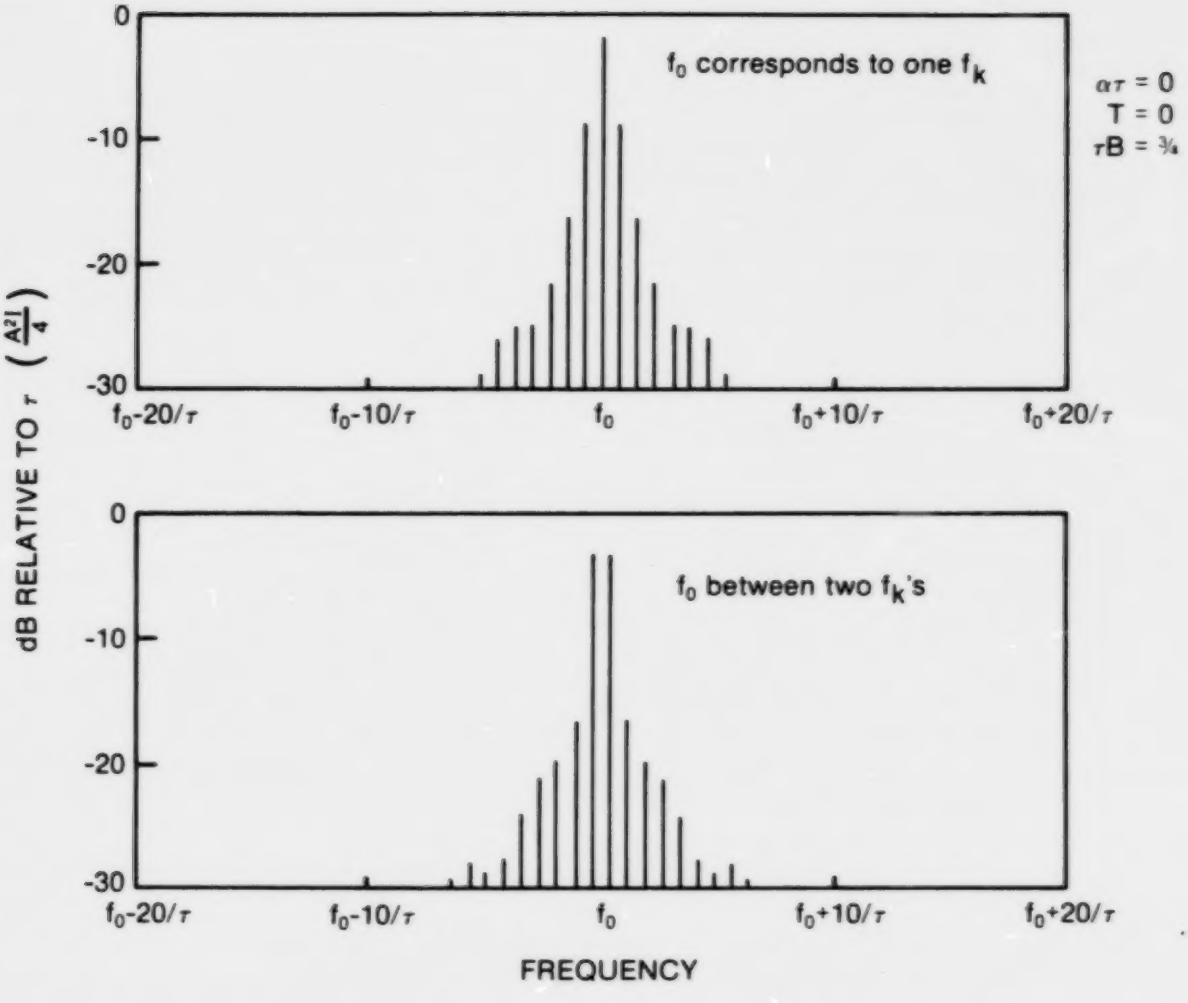

FIGURE 14 - OUTPUT OF AOSA FOR $\alpha\tau = 0$, $T = 0$, $\tau B = 3/4$

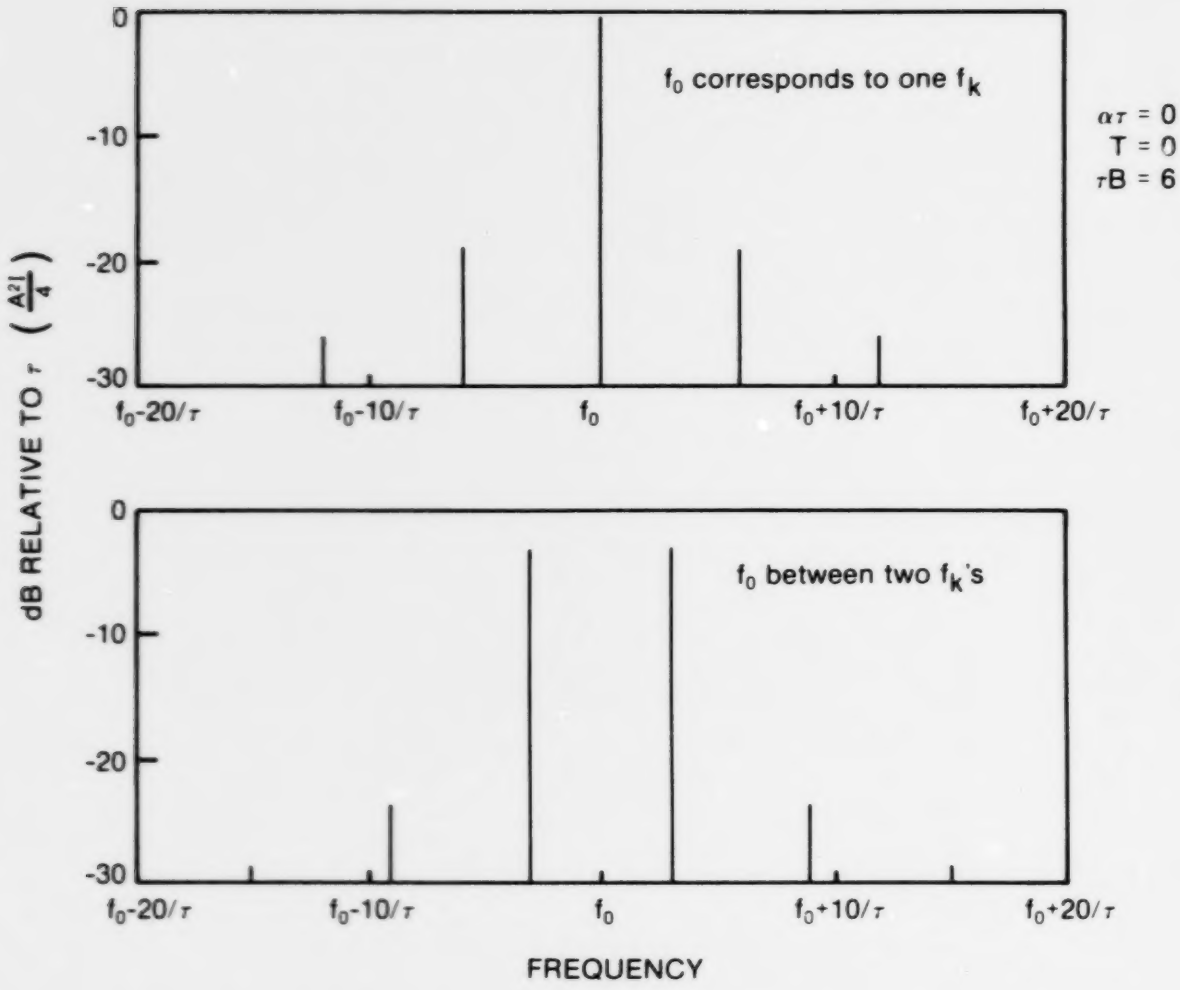

FIGURE 15 - OUTPUT OF AOSA FOR $\alpha\tau = 0$, $T = 0$, $\tau B = 6$

Since in the RESM context we have no a priori knowledge of the probabilities for the occurrence of hypothesis H_0 or H_1, we cannot make use of the Bayes' criterion. If we let P_F be the probability of a false alarm (i.e. the probability that we say the signal is present when it is not) and P_D the probability of detection (i.e. the probability that we say the signal is present when it is), then an obvious criterion would be to constrain P_F and design a test that will maximize P_D. This is known as the Neyman-Pearson criterion and it is shown in [7] that it is satisfied by the likelihood ratio test

$$\Lambda(\bar{R}) \underset{H_0}{\overset{H_1}{\gtrless}} \lambda \tag{17}$$

where the likelihood ratio is defined as

$$\Lambda(\bar{R}) \equiv \frac{p(\bar{R} \mid H_1)}{p(\bar{R} \mid H_0)} \tag{18}$$

where $p(\bar{R} \mid H_i)$ is the conditional probability of the received vector $\bar{R}$ given that hypothesis H_i is true and where λ is defined by the following equation:

$$P_F = \int_{\lambda}^{\infty} p(\Lambda(\bar{R}) \mid H_0) d\Lambda(\bar{R}) \tag{19}$$

It is easy to show that for our problem as it is defined in equation (15), the above conditional probabilities are as follows:

$$p(\bar{R} \mid H_0) = \prod_{i=1}^{N} \frac{1}{\sqrt{2\pi\sigma^2}} \exp\left(\frac{-r_i^2}{2\sigma^2}\right) \tag{20}$$

$$p(\bar{R} \mid H_1) = \prod_{i=1}^{N} \frac{1}{\sqrt{2\pi\sigma^2}} \exp\left[\frac{-(r_i - m_i)^2}{2\sigma^2}\right] \tag{21}$$

hence the likelihood function can be written as

$$\Lambda(\bar{R}) = \exp\left[\frac{\sum_{i=1}^{N} r_i^2 - \sum_{i=1}^{N}(r_i - m_i)^2}{2\sigma^2}\right] \tag{22}$$

or even as

$$\Lambda(\bar{R}) = \exp\left(\frac{2\sum_{i=1}^{N} r_i m_i - \sum_{i=1}^{N} m_i^2}{2\sigma^2}\right) \tag{23}$$

But because the natural logarithm is a monotonic function and both sides of equation (17) must be positive, the likelihood ratio test is equivalent to the test

$$ln\{\Lambda(\bar{R})\} \underset{H_0}{\overset{H_1}{\gtrless}} ln(\lambda) \tag{24}$$

which is very useful given the form of $\Lambda(\bar{R})$ as shown in equation (23).

Indeed, we can say that a test satisfying the Neyman-Pearson criterion for our problem is as follows:

$$\frac{2\sum_{i=1}^{N} r_i m_i - \sum_{i=1}^{N} m_i^2}{2\sigma^2} \underset{H_0}{\overset{H_1}{\gtrless}} ln(\lambda) \tag{25}$$

which is equivalent to the test

$$\sum_{i=1}^{N} r_i m_i \underset{H_0}{\overset{H_1}{\gtrless}} \gamma \tag{26}$$

where γ is a constant.

It should be noted that hypothesis H_1 is a composite hypothesis because it contains the "unwanted" parameter, A and the test of equation (26) cannot be used unless we know the value of A. However, since $m_i = \frac{A^2 I}{4}\mathcal{H}_i$, we can reduce the above test to the following:

$$\sum_{i=1}^{N} r_i \mathcal{H}_i \underset{H_0}{\overset{H_1}{\gtrless}} \gamma' \tag{27}$$

because $A^2 I$ is a positive quantity. If we let $Y = \sum_{i=1}^{N} r_i \mathcal{H}_i$, then the above test becomes

$$Y \underset{H_0}{\overset{H_1}{\gtrless}} \gamma' \tag{28}$$

and

$$P_F = \int_{\gamma'}^{\infty} p(Y \mid H_0) dy \tag{29}$$

The above test is what is called a "uniformly most powerful" (UMP) test because it is completely defined (including threshold) without knowledge of the parameter "A", which is the amplitude of the input signal. Of course, the performance of this test will be a function of this parameter, as will be shown shortly.

In order to find the performance of this test, we note that if H_0 is true, then Y is a Gaussian random variable with zero mean and variance $\sigma_Y^2 = \sigma^2 \sum_{i=1}^{N} \mathcal{H}_i^2$. And similarly, if H_1 is true, then Y is a Gaussian random variable with mean, $\bar{Y} = \sum_{i=1}^{N} m_i \mathcal{H}_i = \frac{A^2 I}{4} \sum_{i=1}^{N} \mathcal{H}_i^2$ and variance, $\sigma_Y^2 = \sigma^2 \sum_{i=1}^{N} \mathcal{H}_i^2$. From this we have that

$$P_F = \int_{\gamma'}^{\infty} \frac{1}{\sigma_Y \sqrt{2\pi}} \exp\left(\frac{-x^2}{2\sigma_Y^2}\right) dx \tag{30}$$

or

$$P_F = erfc\left(\frac{\gamma'}{\sigma_Y}\right) \tag{31}$$

where

$$erfc(t) \equiv \int_t^\infty \frac{1}{\sqrt{2\pi}} \exp\left(\frac{-x^2}{2}\right) dx \tag{32}$$

and

$$P_D = \int_{\gamma'}^\infty \frac{1}{\sqrt{2\pi}\sigma_Y} \exp\left[\frac{-(x-\bar{Y})^2}{2\sigma_Y^2}\right] dx \tag{33}$$

or

$$P_D = erfc\left(\frac{\gamma' - \bar{Y}}{\sigma_Y}\right) \tag{34}$$

Or if we use the error function notation of the IMSL library we have that:

$$P_F = \frac{1}{2} erfc_{IMSL}\left(\frac{\gamma'}{\sqrt{2}\sigma_Y}\right) \tag{35}$$

and

$$P_D = \frac{1}{2} erfc_{IMSL}\left(\frac{\gamma' - \bar{Y}}{\sqrt{2}\sigma_Y}\right) \tag{36}$$

where

$$erfc_{IMSL}(t) = \frac{2}{\sqrt{\pi}} \int_t^\infty \exp(-t^2) dt \tag{37}$$

Figure 16 shows the performance of the test of equation (27) as a function of the parameter

$$x = \frac{A^2 I}{\sigma} \sqrt{\sum_{i=1}^{N} \mathcal{H}_i^2}$$

which serves as a figure of merit. Indeed x is the S/N ratio times the integration time of the photodetectors(I) times a factor which quantifies the performance gain due to the matched filter. We can see that the performance gain due to the matched filter depends on the number of pixels that are used in the algorithm.

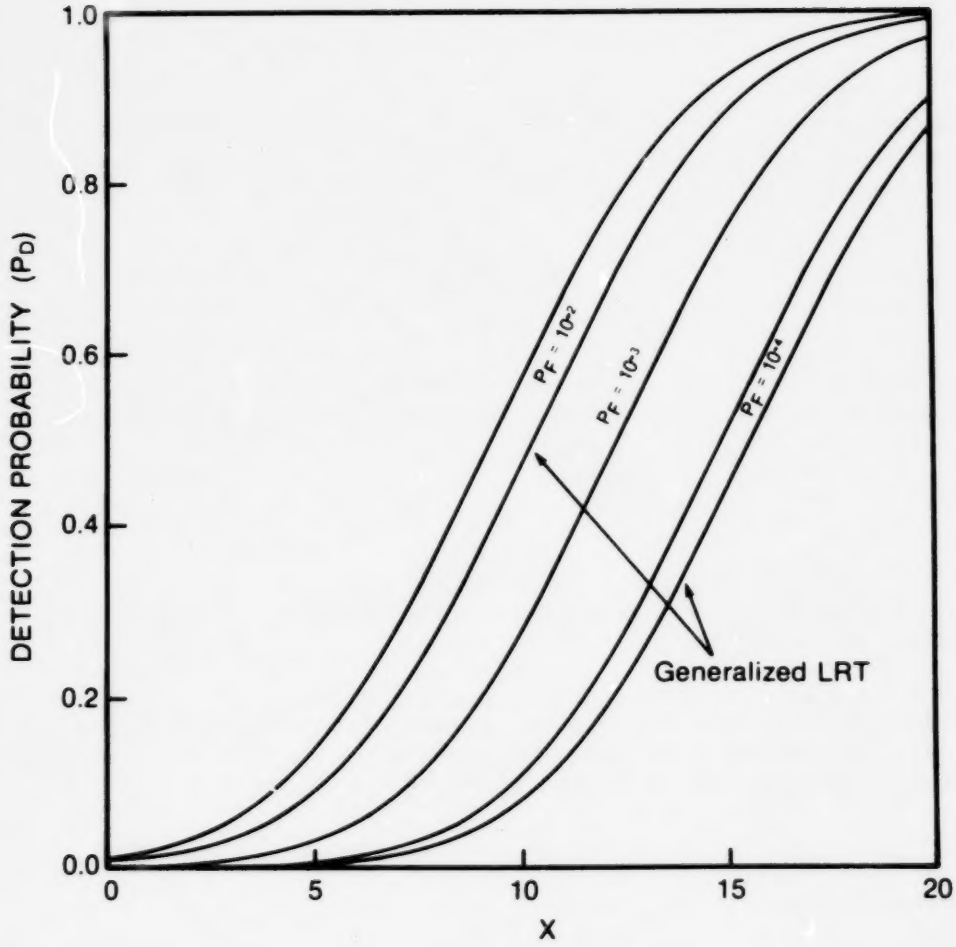

FIGURE 16 - PERFORMANCE CURVE

One would like to know how the performance of the test of equation (27) is affected when the $\mathcal{H}_i$'s used in the test are different from the $\mathcal{H}_i$'s that correspond to the signal. This could happen when the frequency of the input signal is different from the one we assumed or when the signal is actually a short pulse or when the window function, $w(z)$, that we used to calculate the $\mathcal{H}_i$'s was not accurately measured or when the model used to calculate the $\mathcal{H}_i$'s does not accurately represent the processing of the AO processor or for any other reason.

To calculate this performance degradation, let

$$\tilde{Y} = \sum_{i=1}^{N} r_i \tilde{\mathcal{H}}_i \underset{H_0}{\overset{H_1}{\gtrless}} \gamma' \tag{38}$$

be the test, where the $\tilde{\mathcal{H}}_i$'s are used in the test but do not actually correspond to the $\mathcal{H}_i$'s of the signal. In this case, if H_0 is true, $\tilde{Y}$ is a Gaussian random variable with zero mean and variance $\sigma_{\tilde{Y}}^2 = \sigma^2 \sum_{i=1}^{N} \tilde{\mathcal{H}}_i^2$. But if H_1 is true, then $\tilde{Y}$ is a random variable with mean

$$E\{\tilde{Y}\} = \sum_{i=1}^{N} \tilde{\mathcal{H}}_i m_i = \frac{A^2 I}{4} \sum_{i=1}^{N} \tilde{\mathcal{H}}_i \mathcal{H}_i$$

and variance $\sigma_{\tilde{Y}}^2 = \sigma^2 \sum_{i=1}^{N} \tilde{\mathcal{H}}_i^2$. It is easy to show that the performance of the test of equation (38) is the same as the performance of the UMP test as shown in Figure 16 except that for this case

$$x = \frac{A^2 I \sum_{i=1}^{N} \tilde{\mathcal{H}}_i \mathcal{H}_i}{\sigma \sqrt{\sum_{i=1}^{N} \tilde{\mathcal{H}}_i^2}}$$

and hence the performance degradation is determined by the term $\sum_{i=1}^{N} \tilde{\mathcal{H}}_i \tilde{H}_i$ which can be seen as a figure of merit to evaluate the degradation of the proposed test.

It should be noted, in concluding this section, that in the RESM context one has no a priori knowledge of the frequency of the input signal. However, one could use the proposed test to decide on the presence of many different frequencies. This could be done by using an FIR filter where the tap coefficients are matched to the $\mathcal{H}_i$'s that are expected, the implementation of which is discussed in [8].

3.2 Power Estimation

As it was mentioned in section 3.1, hypothesis H_1 is a composite hypothesis because it contains the unknown parameter "A", which is the amplitude of the input signal (c.f. equations (15) and (16)). However, it is possible to estimate the value of the parameter "A" from the r_i's of the received vector $\bar{R}$. But since the power of the input signal is usually of more interest than the amplitude, we will estimate "A^2".

There are many algorithms that could be used to estimate "A^2", however, one that has an important property is the maximum-likelihood (ML) estimate. Indeed, it is mentioned in [9] that if the maximum-likelihood estimate is unbiased, then it will satisfy the Cramér-Rao bound with an equality. An estimator which satisfies the Cramér-Rao bound with an equality is known in the literature as an *efficient* estimator.

Now to find the ML estimate for A^2 we must solve,

$$\frac{\partial ln\left\{p(\bar{R}|A^2)\right\}}{\partial A^2} = 0 \tag{39}$$

Substituting equation (21) in equation (39) and simplifying gives us that

$$\frac{\partial \sum_{i=1}^{N}(r_i - m_i)^2/2\sigma^2}{\partial A^2} = 0 \tag{40}$$

Substituting the m_i's gives us

$$\frac{\partial \sum_{i=1}^{N}\left(\frac{A^2 I}{4}\mathcal{H}_i - r_i\right)^2}{\partial A^2} = 0 \tag{41}$$

Differentiating and simplifying we obtain

$$\sum_{i=1}^{N}\left(\frac{I\mathcal{H}_i^2}{4}A^2 - r_i\mathcal{H}_i\right) = 0 \tag{42}$$

From which we get the desired ML estimate:

$$A^2_{ML} = \frac{4}{I}\frac{\sum_{i=1}^{N} r_i\mathcal{H}_i}{\sum_{i=1}^{N}\mathcal{H}_i^2} \tag{43}$$

If we seek to find the mean of the ML estimate, we have that

$$E\left\{A^2_{ML}\right\} = E\left\{\frac{4\sum_{i=1}^{N} r_i\mathcal{H}_i}{I\sum_{i=1}^{N}\mathcal{H}_i^2}\right\} \tag{44}$$

which becomes

$$E\left\{A^2_{ML}\right\} = \frac{4}{I\sum_{i=1}^{N}\mathcal{H}_i^2}\sum_{i=1}^{N}(\mathcal{H}_i E\{r_i\}) \tag{45}$$

which can easily be calculated to be

$$E\left\{A^2_{ML}\right\} = A^2 \tag{46}$$

Hence we see that the ML estimate is unbiased and we can therefore conclude that it is an efficient estimate of the parameter A^2. That is, it is impossible to find an other unbiased estimate of A^2 which has a smaller variance than the ML estimate of A^2.

Of course, we could use our estimate of A^2 to calculate the likelihood ratio of equation (26) and therefore obtain what is called a generalized likelihood ratio test. However, this would not be a good thing to do since we were able to obtain a UMP test for this problem and the generalized likelihood ratio test is bound to have a poorer performance.

However, for sake of completeness, it can be shown that the generalized likelihood ratio becomes:

$$(Y_g)^2 \underset{H_0}{\overset{H_1}{\gtrless}} \gamma_g^2 \tag{47}$$

where γ_g^2 is a constant and $Y_g = \sum_{i=1}^{N} r_i \mathcal{H}_i$. It can further be shown that the performance of this test is such that

$$P_D = erfc\left(\frac{\gamma_g - \bar{Y}_g}{\sigma_{Y_g}}\right) + erf\left(\frac{-\gamma_g - \bar{Y}_g}{\sigma_{Y_g}}\right) \tag{48}$$

and

$$P_F = 2 \cdot erfc\left(\frac{\gamma_g}{\sigma_{Y_g}}\right) \tag{49}$$

where $\bar{Y}_g$ is the mean of Y_g and $\sigma_{Y_g}^2$ is the variance of Y_g. Figure 16 also shows the performance of that test where again

$$x = \frac{A^2 I}{\sigma}\sqrt{\sum_{i=1}^{N} \mathcal{H}_i^2}$$

as for the UMP test.

3.3 Carrier Frequency Estimation

In section 3.1 it was mentioned that, in the RESM context, we have no a priori knowledge of the probabilities for the occurrence of hypothesis H_0 or H_1. But even worst than that, we also don't have any a priori knowledge of the probability distribution function for the carrier frequency of the input signals. However, if we are given that a signal is present, we can express the likelihood function as

$$P(\bar{R}|f_0) = \prod_{i=1}^{N} \frac{1}{\sqrt{2\pi\sigma^2}} \exp\left\{\frac{(r_i - m_i)^2}{2\sigma^2}\right\} \tag{50}$$

where the frequency dependence rests upon the m_i's which are assumed to be known for different carrier frequencies, f_0. Or to simplify the calculations, we can obtain the log likelihood function which is

$$-N\ln(\sqrt{2\pi}\sigma^2) - \sum_{i=1}^{N} \frac{(r_i - m_i)^2}{2\sigma^2} \tag{51}$$

By definition, the ML estimator of the carrier frequency is the frequency that will maximize equation (51). But since, in general, there exists no closed form expression for the m_i's, it is not possible to get an expression for the ML estimator. One way to counter this problem is to substitute the m_i's which correspond to all the possible frequencies in equation (51) and note which frequency actually maximized it. If there are an infinity of possible frequencies, then instead we can separate the range of frequencies in a number of bins which form a fine mesh over that range. In that case, the number of bins could be determined by such factors as the frequency resolution desired or the computing power available or affordable.

It is clear that equation (51) is maximized when

$$\left|\bar{R} - \bar{M}\right|^2 = |\bar{R}|^2 + |\bar{M}|^2 - 2\langle \bar{R}, \bar{M} \rangle \tag{52}$$

is minimized. In general, $|\bar{M}|^2$ is not constant for all frequencies but is periodic with period B, which is the bandwidth covered by one photodetector. Hence, if we calculate equation (52) for a set of frequencies which are separated in frequency by multiples of B, then equation (52) will reach a minimum when the term $\langle \bar{R}, \bar{\mathcal{H}} \rangle$ reaches a maximum. This is an interesting result in light of the fact that this term corresponds to the UMP detection test that was obtained in section 3.1.

Indeed, a block diagram of a system to detect the presence of signals and estimate the carrier frequency of those signals could be as shown in Figure 17. The matched filter could be implemented by an FIR filter where the tap coefficients are the calculated $\mathcal{H}_i$'s. If many different types of signals could be present, we could select a filter which gives the smallest overall degradation by using the result obtained in section 3.1. The output of the matched filter can be compared with a threshold comparator to decide if a signal is present or not. And finally, of all the outputs of the FIR filter which are above the threshold, the highest one could be used to estimate the carrier frequency of the input signal. It should be noted that the peak detector block should also have the capability of recognizing more than one signal per integration frame which could often be the case for this application.

4.0 CONCLUDING REMARKS

We have discussed the modelling and processing of the signals from an AOSA. The modelling has been done for CW signals but we have shown that it can be applied to pulse modulated signals as well. The case of biphase coded signals has not been addressed. The analysis has been kept general as much as possible so that the results can be tailored to specific systems. We have proposed the block diagram of a system that could be used to detect and estimate the carrier frequency of an input radar signal.

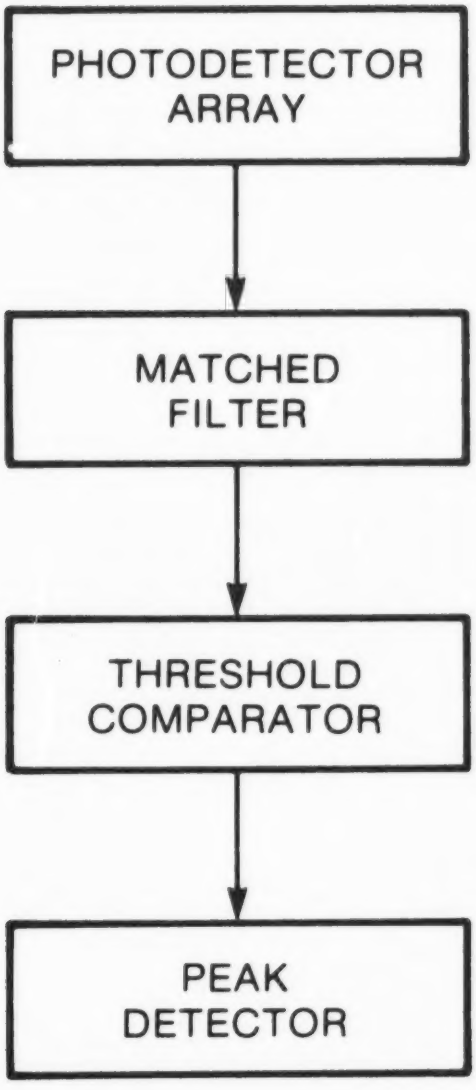

FIGURE 17 - DETECTION/ESTIMATION SYSTEM

5.0 REFERENCES

[1] Lee, Jim P.Y., 'Acoustooptic Spectrum Analysis of Radar Signals Using an Integrating Photodetector Array', *Applied Optics*, Vol. 20, No. 4, pp. 595-600, February 15, 1981.

[2] Vander Lugt, A., 'Bragg Cell Diffraction Patterns', *Applied Optics*, Vol. 21, No. 6, pp. 1092-1100, March 15, 1982.

[3] Kellman, Peter, et. al., 'Integrating Acousto-Optic Channelized Receivers', *Proceedings of the IEEE*, Vol. 69, No. 1, pp. 93-100, January 1981.

[4] Harms, B.K. and Hummels, D.R., 'Analysis of Detection Probability for the Acoustooptic Receiver', *IEEE transactions on Aerospace and Electronic Systems*, Vol. AES-22, No. 4, pp. 326-339, July 1986.

[5] Hecht, D.L., 'Spectrum Analysis Using Acousto-Optic Devices', *Optical Engineering*, Vol. 16, No. 5, pp. 461-466, September/October 1977.

[6] Heideman, Michael T., et. al., 'Gauss and the History of the Fast Fourier Transform', *IEEE ASSP Magazine*, Vol. 1, No. 4, pp. 14-21, October 1984.

[7] Van Trees, Harry L., *Detection, Estimation, and Modulation Theory, Part I*, New York: Wiley, 1968.

[8] Inkol, Robert J., Farley, Guy, 'Post Processor Design Concepts Applicable to an Acousto Optic Spectrum Analyzer (U)', Unclassified, Technical Note, *DREO TN 87-2*, January 1987.

[9] Haykin, S., et. al., *Array Signal Processing*, pp. 208, Prentice-Hall, 1984.

APPENDIX I

CALCULATION OF X_{jk} FOR A CW INPUT

We have defined,

$$X_{jk} = \int_{jI}^{(j+1)I} \int_{-\infty}^{\infty} H(f - f_k) \left| \int_{-\infty}^{\infty} w(\beta) u(t - \beta) \exp(-i2\pi f \beta) d\beta \right|^2 df\, dt \qquad (I-1)$$

which can be rewritten

$$X_{jk} = \int_{jI}^{(j+1)I} \int_{-\infty}^{\infty} \int_{-\infty}^{\infty} \int_{-\infty}^{\infty} H(f - f_k) w(\alpha) w^*(\beta) u(t - \alpha) u^*(t - \beta) \exp[-i2\pi f(\alpha - \beta)]\, d\alpha\, d\beta\, df\, dt \qquad (I-2)$$

Now, if

$$u(t) = A \cos(2\pi f_0 t + \phi) \qquad (I-3)$$

then

$$u(t - \alpha) u^*(t - \beta) = A \cos[2\pi f_0 (t - \alpha) + \phi] \cdot A \cos[2\pi f_0 (t - \beta) + \phi] \qquad (I-4)$$

which can be rewritten as

$$\frac{A^2}{2} \left\{ \cos[4\pi f_0 t - 2\pi f_0 (\alpha + \beta) + 2\phi] + \cos[2\pi f_0 (\alpha - \beta)] \right\} \qquad (I-5)$$

Hence,

$$X_{jk} = \frac{A^2}{2} \int_{jI}^{(j+1)I} \int_{-\infty}^{\infty} \int_{-\infty}^{\infty} \int_{-\infty}^{\infty} H(f - f_k) w(\alpha) w^*(\beta) \left\{ \cos[2\pi f_0 (\alpha - \beta)] + \cos[4\pi f_0 t - 2\pi f_0 (\alpha + \beta) + 2\phi] \right\} \exp[-i2\pi f(\alpha - \beta)]\, d\alpha\, d\beta\, df\, dt \qquad (I-6)$$

or

$$X_{jk} = \frac{A^2}{2} \int_{-\infty}^{\infty} \int_{-\infty}^{\infty} \int_{-\infty}^{\infty} H(f - f_k) w(\alpha) w^*(\beta) \exp[-i2\pi f(\alpha - \beta)] \int_{jI}^{(j+1)I} \left\{ \cos[2\pi f_0 (\alpha - \beta)] + \cos[4\pi f_0 t - 2\pi f_0 (\alpha + \beta) + 2\phi] \right\} dt\, d\alpha\, d\beta\, df \qquad (I-7)$$

Now,

$$\exp[-i2\pi f(\alpha-\beta)]\int_{jI}^{(j+1)I}\Big\{\cos[2\pi f_0(\alpha-\beta)]+\cos[4\pi f_0 t-2\pi f_0(\alpha+\beta)+2\phi]\Big\}dt$$

$$=\exp[-i2\pi f(\alpha-\beta)]\Big\{\cos[2\pi f_0(\alpha-\beta)]\,I$$

$$+\left[\frac{\sin[4\pi f_0 t-2\pi f_0(\alpha+\beta)+2\phi]}{4\pi f_0}\right]_{jI}^{(j+1)I}\Big\} \quad (I-8)$$

which if $I \gg 1/4\pi f_0$

$$\approx \exp[-i2\pi f(\alpha-\beta)]\cos[2\pi f_0(\alpha-\beta)]\,I \quad (I-9)$$

Now we should note that

$$\exp[-i2\pi f(\alpha-\beta)]\cos[2\pi f_0(\alpha-\beta)]\,I$$

$$=\frac{I}{2}\exp[-i2\pi f(\alpha-\beta)]\Big\{\exp[i2\pi f_0(\alpha-\beta)]+\exp[-i2\pi f_0(\alpha-\beta)]\Big\}$$

$$=\frac{I}{2}\Big\{\exp[-i2\pi(\alpha-\beta)(f-f_0)]+\exp[-i2\pi(\alpha-\beta)(f+f_0)]\Big\} \quad (I-10)$$

Substituting (I-10) in (I-7) we get

$$X_{jk}\approx\frac{A^2I}{4}\int_{-\infty}^{\infty}\int_{-\infty}^{\infty}\int_{-\infty}^{\infty}H(f-f_k)w(\alpha)w^*(\beta)\Big\{\exp[-i2\pi(\alpha-\beta)(f-f_0)]$$

$$+\exp[-i2\pi(\alpha-\beta)(f+f_0)]\Big\}d\alpha\,d\beta\,df \quad (I-11)$$

If we define

$$G(f)\equiv\left|\int_{-\infty}^{\infty}w(z)\exp(-i2\pi fz)dz\right|^2 \quad (I-12)$$

which is the magnitude squared of the Fourier transformed window function, then we can rewrite

$$G(f)=\int_{-\infty}^{\infty}w(\alpha)\exp(-i2\pi f\alpha)d\alpha\int_{-\infty}^{\infty}w^*(\beta)\exp(i2\pi f\beta)d\beta$$

$$=\int_{-\infty}^{\infty}\int_{-\infty}^{\infty}w(\alpha)w^*(\beta)\exp(-i2\pi f\alpha)\exp(i2\pi f\beta)d\alpha\,d\beta$$

$$=\int_{-\infty}^{\infty}\int_{-\infty}^{\infty}w(\alpha)w^*(\beta)\exp[-i2\pi f(\alpha-\beta)]\,d\alpha\,d\beta \quad (I-13)$$

and hence

$$G(f+f_0)=\int_{-\infty}^{\infty}\int_{-\infty}^{\infty}w(\alpha)w^*(\beta)\exp\left[-i2\pi(\alpha-\beta)(f+f_0)\right]d\alpha\,d\beta \qquad (I-14)$$

and similarly

$$G(f-f_0)=\int_{-\infty}^{\infty}\int_{-\infty}^{\infty}w(\alpha)w^*(\beta)\exp\left[-i2\pi(\alpha-\beta)(f-f_0)\right]d\alpha\,d\beta \qquad (I-15)$$

Substituting (I-14) and (I-15) in (I-11) we get

$$X_{jk}\approx\frac{A^2I}{4}\int_{-\infty}^{\infty}H(f-f_k)\left[G(f-f_0)+G(f+f_0)\right]df \qquad (I-16)$$

Now if we assume that $H(f)$ is symmetrical about $f=0$, then

$$\begin{aligned}\int_{-\infty}^{\infty}H(f-f_k)G(f+f_0)df&=\int_{-\infty}^{\infty}H(f_k-f)G(f+f_0)df\\&=\int_{-\infty}^{\infty}H\left[f_k-(f+f_0)+f_0\right]G(f+f_0)df\\&=\int_{-\infty}^{\infty}H(f_k+f_0-f')G(f')df'=\mathcal{H}(f_k+f_0)\end{aligned} \qquad (I-17)$$

where,

$$\mathcal{H}(f)=\int_{-\infty}^{\infty}H(f-f')G(f')df' \qquad (I-18)$$

which is the convolution between the functions G and H. And similarly, it can be shown that

$$\mathcal{H}(f_k-f_0)=\int_{-\infty}^{\infty}H(f-f_k)G(f-f_0)df \qquad (I-19)$$

Hence, substituting (I-17) and (I-19) in (I-16) we get that

$$X_{jk}\approx\frac{A^2I}{4}\left\{\mathcal{H}(f_k-f_0)+\mathcal{H}(f_k+f_0)\right\} \qquad (I-20)$$

But $\mathcal{H}(f_k+f_0)$ is very small compared to $\mathcal{H}(f_k-f_0)$ for large values of f_k or f_0, hence

$$X_{jk}\approx\frac{A^2I}{4}\mathcal{H}(f_k-f_0) \qquad (I-21)$$

APPENDIX II

NUMERICAL CALCULATION OF $G(f)$ FOR THE GENERAL CASE

From equation (5) we have that

$$w(z) = \exp\left[-\alpha z - 4T^2\left(\frac{z}{\tau} - \frac{1}{2}\right)^2\right] \text{rect}\left(\frac{z}{\tau} - \frac{1}{2}\right) \qquad (II-1)$$

or we could normalize $w(z)$ and get

$$w(x) = \exp\left[-Lx - 4T^2\left(x - \frac{1}{2}\right)^2\right] \text{rect}\left(x - \frac{1}{2}\right) \qquad (II-2)$$

where $L = \alpha\tau$ and $x = \frac{t}{\tau}$.

From equation (4) and (II-1) we have that

$$G(f) = \left|\int_0^\tau w(z)\exp(-i2\pi f z)dz\right|^2 \qquad (II-3)$$

A closed form solution to this equation does not exist in general unless some simplification or approximation is done. The rectangular rule can provide a numerical estimate of this integration. This gives the following equation as an estimate of equation (II-3):

$$G_a(f) = \left|\Delta t \sum_{n=0}^{N-1} w(n\Delta t)\exp(-i2\pi f n\Delta t)\right|^2 \qquad (II-4)$$

Now, in this case we will let $\Delta t = \tau/N$ where N is the number of points from $w(z)$ that will be used to calculate one sample of $G(f)$.

Replacing $\Delta t = \tau/N$ in (II-4) we have:

$$G_a(f) = \left|\frac{\tau}{N}\sum_{n=o}^{N-1} w\left(\frac{n\tau}{N}\right)\exp\left(\frac{-i2\pi f n\tau}{N}\right)\right|^2 \qquad (II-5)$$

if we let $v = f\tau$ we get

$$G_a(v) = \left|\frac{\tau}{N}\sum_{n=0}^{N-1} w\left(\frac{n\tau}{N}\right)\exp\left(\frac{-i2\pi v n}{N}\right)\right|^2 \qquad (II-6)$$

or if we express the above equation in rectangular coordinates, we get

$$G_a(v) = |\tau K|^2 \qquad (II-7)$$

where,

$$K = \frac{\sum_{n=0}^{N-1} \left[w\left(\frac{n\tau}{N}\right) \cos\left(\frac{2\pi\nu n}{N}\right) - iw\left(\frac{n\tau}{N}\right) sin\left(\frac{2\pi\nu n}{N}\right) \right]}{N} \qquad (II-8)$$

hence,

$$G_a(\nu) = \tau^2 \left\{ [Re(K)]^2 + [Im(K)]^2 \right\} \qquad (II-9)$$

To consider the error associated with the approximation of (II-9) let

$$X_a(f) = \Delta t \sum_{n=0}^{N-1} w(n\Delta t) \exp(-i2\pi f n\Delta t) \qquad (II-10)$$

It is easy to see from (II-4) that

$$G_a(f) = |X_a(f)|^2 \qquad (II-11)$$

We note that the Fourier transform of a delayed Dirac delta function, $\delta(t - t_0)$, is $e^{-i2\pi f t_0}$. Thus we may regard (II-10) as the Fourier transform of $\Delta t \sum_{n=0}^{N-1} w(n\Delta t)\delta(t - n\Delta t)$:

$$X_a(f) = \mathcal{F}\left\{ \Delta t \sum_{n=0}^{N-1} w(n\Delta t)\delta(t - n\Delta t) \right\} \qquad (II-12)$$

Since $w(z)$ is zero outside the interval $[0, \tau]$, we may rewrite (II-12) as

$$X_a(f) = \mathcal{F}\left\{ w(z) \cdot \Delta t \sum_{n=-\infty}^{\infty} \delta(z - n\Delta t) \right\} \qquad (II-13)$$

which can be transformed, using the well known property for the Fourier transform of multiplied time functions, to the following:

$$X_a(f) = W(f) * \mathcal{F}\left\{ \Delta t \sum_{n=-\infty}^{\infty} \delta(t - n\Delta t) \right\}$$

which becomes

$$X_a(f) = W(f) * \sum_{m=-\infty}^{\infty} \delta\left(f - \frac{m}{\Delta t}\right)$$

which finally becomes

$$X_a(f) = \sum_{n=-\infty}^{\infty} W\left(f - \frac{n}{\Delta t}\right) \qquad (II-14)$$

So we see that the approximation of equation (II-9) is in fact an aliased version of $G(f)$. We also see that $G_a(f)$ is periodic with period $1/\Delta t$, hence there is no point in calculating $G_a(f)$ outside the range of frequencies

$$\frac{-N}{2\tau} < f < \frac{N}{2\tau}$$

since $\Delta t = \tau/N$. Or if we use the normalized version $G_a(v)$, then the range of frequencies is

$$\frac{-N}{2} < v < \frac{N}{2}$$

SECURITY CLASSIFICATION OF FORM
(highest classification of Title, Abstract, Keywords)

DOCUMENT CONTROL DATA

(Security classification of title, body of abstract and indexing annotation must be entered when the overall document is classified)

1. ORIGINATOR (the name and address of the organization preparing the document. Organizations for whom the document was prepared, e.g. Establishment sponsoring a contractor's report, or tasking agency, are entered in section 8.)

DEFENCE RESEARCH ESTABLISHMENT OTTAWA
DEPARTMENT OF NATIONAL DEFENCE
SHIRLEY BAY, OTTAWA, ONTARIO K1A 0Z4 CANADA

2. SECURITY CLASSIFICATION (overall security classification of the document including special warning terms if applicable)

UNCLASSIFIED

3. TITLE (the complete document title as indicated on the title page. Its classification should be indicated by the appropriate abbreviation (S,C,R or U) in parentheses after the title.)

DISCUSSION ON THE MODELLING AND PROCESSING OF SIGNALS FROM AN ACOUSTO-OPTIC SPECTRUM ANALYZER (U)

4. AUTHORS (Last name, first name, middle initial. If military, show rank, e.g. Doe, Maj. John E.)

FARLEY, GUY J.

5. DATE OF PUBLICATION (month and year of publication of document)

JUNE 1987

6a. NO. OF PAGES (total containing information. Include Annexes, Appendices, etc.)

39

6b. NO. OF REFS (total cited in document)

9

7. DESCRIPTIVE NOTES (the category of the document, e.g. technical report, technical note or memorandum. If appropriate, enter the type of report, e.g. interim, progress, summary, annual or final. Give the inclusive dates when a specific reporting period is covered.)

DREO TECHNICAL NOTE 87-13

8. SPONSORING ACTIVITY (the name of the department project office or laboratory sponsoring the research and development. Include the address.)

9a. PROJECT OR GRANT NO. (if appropriate, the applicable research and development project or grant number under which the document was written. Please specify whether project or grant)

011LB11

9b. CONTRACT NO. (if appropriate, the applicable number under which the document was written)

10a. ORIGINATOR'S DOCUMENT NUMBER (the official document number by which the document is identified by the originating activity. This number must be unique to this document.)

10b. OTHER DOCUMENT NOS. (Any other numbers which may be assigned this document either by the originator or by the sponsor)

DRP 87-326

11. DOCUMENT AVAILABILITY (any limitations on further dissemination of the document, other than those imposed by security classification)

(X) Unlimited distribution
( ) Distribution limited to defence departments and defence contractors; further distribution only as approved
( ) Distribution limited to defence departments and Canadian defence contractors; further distribution only as approved
( ) Distribution limited to government departments and agencies; further distribution only as approved
( ) Distribution limited to defence departments; further distribution only as approved
( ) Other (please specify):

12. DOCUMENT ANNOUNCEMENT (any limitation to the bibliographic announcement of this document. This will normally correspond to the Document Availabilty (11). However, where further distribution (beyond the audience specified in 11) is possible, a wider announcement audience may be selected.)

UNCLASSIFIED

SECURITY CLASSIFICATION OF FORM

13. ABSTRACT (a brief and factual summary of the document. It may also appear elsewhere in the body of the document itself. It is highly desirable that the abstract of classified documents be unclassified. Each paragraph of the abstract shall begin with an indication of the security classification of the information in the paragraph (unless the document itself is unclassified) represented as (S), (C), (R), or (U). It is not necessary to include here abstracts in both official languages unless the text is bilingual).

(U) This report discusses, in its first part, the modeling of CW signals generated by an Acousto-Optic Spectrum Analyzer (AOSA). It also shows how this calculation can be related to pulse modulated signals. In its second part, it discusses the processing of those signals to detect and to estimate the carrier frequency and the power of an input radar signal. It also proposes a system block diagram to implement the former two functions.

14. KEYWORDS, DESCRIPTORS or IDENTIFIERS (technically meaningful terms or short phrases that characterize a document and could be helpful in cataloguing the document. They should be selected so that no security classification is required. Identifiers, such as equipment model designation, trade name, military project code name, geographic location may also be included. If possible, keywords should be selected from a published thesaurus. e.g. Thesaurus of Engineering and Scientific Terms (TEST) and that thesaurus identified. If it is not possible to select indexing terms which are Unclassified, the classification of each should be indicated as with the title.)

Modeling
Processing
Detection
Estimation
Acousto-optic
Spectrum Analysis